Journal Pre-proof

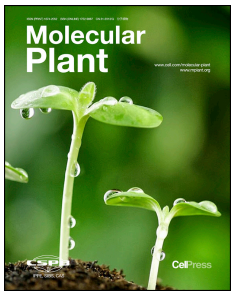

Natural variations in the promoter of *ZmDeSI2* encoding a deSUMOylating isopeptidase control kernel methionine content in maize

Xin Lu, Yuhong Lei, Zhennan Xu, Zixiang Cheng, Meng Liu, Yuxin Tai, Xiaohua Han, Zhuanfang Hao, Mingshun Li, Degui Zhang, Hongjun Yong, Jienan Han, Zhenhua Wang, Wenxue Li, Jianfeng Weng, Zhiqiang Zhou, Xinhai Li

PII: S1674-2052(25)00134-0

DOI: https://doi.org/10.1016/j.molp.2025.04.008

Reference: MOLP 1897

To appear in: *MOLECULAR PLANT*

Received Date: 20 November 2024

Revised Date: 31 March 2025

Accepted Date: 17 April 2025

Please cite this article as: Lu X., Lei Y., Xu Z., Cheng Z., Liu M., Tai Y., Han X., Hao Z., Li M., Zhang D., Yong H., Han J., Wang Z., Li W., Weng J., Zhou Z., and Li X. (2025). Natural variations in the promoter of *ZmDeSI2* encoding a deSUMOylating isopeptidase control kernel methionine content in maize. Mol. Plant. doi: https://doi.org/10.1016/j.molp.2025.04.008.

Title: Natural variations in the promoter of *ZmDeSI2* encoding a deSUMOylating isopeptidase control kernel methionine content in maize

Short Summary

This study identified the deSUMOylating isopeptidase gene *ZmDeSI2* as a key regulator of methionine (Met) content in maize kernels. It was found that ZmDeSI2 suppressed Met accumulation by reducing the SUMOylation of ZmSIR, and identified a presence-absence variant in the *ZmDeSI2* promoter responsible for Met level regulation, offering a target for biofortification in maize breeding.

Authors

Xin Lu [1†], Yuhong Lei[1], Zhennan Xu[1], Zixiang Cheng[1], Meng Liu[1], Yuxin Tai[1], Xiaohua Han[3], Zhuanfang Hao[1], Mingshun Li[1], Degui Zhang[1], Hongjun Yong[1], Jienan Han[1], Zhenhua Wang[2], Wenxue Li[1], Jianfeng Weng[1*], Zhiqiang Zhou[1*], and Xinhai Li[1*]

Affiliations

[1]State Key Laboratory of Crop Gene Resources and Breeding, Institute of Crop Sciences, Chinese Academy of Agricultural Sciences, Beijing, China.

[2]Northeast Agricultural University, Harbin, Heilongjiang, China.

[3]Institute of Food Crops, Henan Academy of Agricultural Sciences, Zhengzhou, Henan, China.

*** Corresponding author**

Xinhai Li, Zhiqiang Zhou, Jianfeng Weng

E-mail: lixinhai@caas.cn; zhouzhiqiang@caas.cn; wengjianfeng@caas.cn

Summary

Efforts to improve the methionine (Met) content in maize kernels are of key importance to the animal feed industry. In this study, a panel consisting of 348 diverse inbred maize lines was leveraged to explore the genetic and molecular mechanisms that govern kernel Met levels. A genome-wide association study ultimately identified the deSUMOylating isopeptidase gene *ZmDeSI2*. In subsequent experiments, *ZmDeSI2* was confirmed to directly reduce the SUMOylation and accumulation of the sulfite reductase ZmSIR, ultimately repressing Met accumulation. Natural variants identified in the *ZmDeSI2* promoter region were found to serve as key determinants of the expression of this gene, with these effects predominantly being attributable to the absence of a ZmWRKY105 transcription factor binding site in *ZmDeSI2*^{Hap2} lines. The artificially selected elite *ZmDeSI2*^{Hap2} haplotype was associated with a 1.36-fold increase in Met levels in the kernels of modified near-isogenic lines generated through marker-assisted breeding based on a presence-absence variation in the *ZmDeSI2* promoter. Together, these results provide new insights into the molecular processes that control Met biosynthesis while also highlighting an elite natural variant suitable for application in maize breeding efforts focused on Met biofortification.

Keywords:

Maize, Methionine, DeSUMOylation, Sulfite reductase, Natural variation

Introduction

Maize is among the most widely produced grains globally, with an estimated output of

1.145 million metric tons in 2024/2025. An estimated 60% of all maize serves as livestock feed (USDA/FAS, Grain: World Markets and Trades, August 2024, https://fas.usda.gov/sites/default/files/2024-08/grain.pdf). However, livestock diets are frequently deficient in essential amino acids, particularly, methionine (Met), tryptophan, and lysine. Met is a primary limiting amino acid in poultry and the second-most important limiting amino acid in swine, and its adequate supply is critical for the efficient utilization of other amino acids. Insufficient Met reduces feed efficiency in both livestock and poultry, increasing nitrogen excretion in the feces and thus contributing to environmental nitrogen pollution (Alagawany et al., 2016). Met deficiency also adversely affects the growth and development of laying hens, resulting in issues such as growth retardation, weight loss, immune suppression, and abnormal liver hypertrophy (Devi et al., 2023). Hen laying rates can be improved by maintaining an optimal 0.4-0.5% dietary Met content (Carvalho et al., 2018); however, the average level of Met in maize is only 0.18-0.23% (Deng et al., 2017). Maize-soybean feed mixtures, commonly used in poultry diets, are deficient in Met as it is also the primary limiting amino acid in soybeans. Overcoming this Met deficiency necessitates the supplemental addition of fish meal and racemic Met when preparing feed, imposing higher costs on the production process (Wang and Wen, 2024). This issue has been particularly problematic in developing countries as it is not economically sustainable and is associated with reduced hen growth rates in some instances (Sveier et al., 2001). Biofortification achieved through the genetic modification of maize to increase kernel Met content, in contrast, holds greater promise for the feed industry (Yan et al., 2023).

The biosynthesis of Met in plants begins with the absorption of sulfate from the soil. A complex process then facilitates its assimilation into various organic compounds (Fuentes-Lara et al., 2019; Kopriva et al., 2019). This process of sulfate uptake from the soil and transport within the plant is coordinated by members of a sulfate transporter family (Hawkesford, 2003). ATP sulfurylase converts sulfate into adenosine 5-phosphosulfate (APS) in plasmids (Herrmann et al., 2014), which is then reduced to sulfite by APS reductase (Jez, 2019), followed by its further reduction to sulfide through a reaction catalyzed by sulfite reductase (SIR) (Kopriva et al., 2019). O-acetylserine sulfhydrylase can then assimilate sulfide into cysteine (Cys), which is incorporated into proteins and glutathione (GSH) to produce homocysteine (Hcy) through the action of Cystathionine *β*-lyase (CBL), with Met synthase (MS) ultimately producing Met (Anjum et al., 2015). Evidence from metabolic studies suggests that there are multiple points responsible for the control of sulfur assimilation. Consistently, maize, tomato (*Solanum lycopersicum*), and *Arabidopsis* plants exhibiting reduced SIR activity present with poorer stress tolerance and a range of growth and developmental abnormalities (Khan et al., 2010; Xia et al., 2018; Yarmolinsky et al., 2014). This suggests that SIR plays a conserved role in S assimilation throughout the plant kingdom. In one recent study, polymorphisms at the SNP69C allele a *ZmSIR* exon were found to post-transcriptionally regulate protein abundance, contributing to the naturally observed variability in Met assimilation (Jiang et al., 2021).

Small ubiquitin-like modification (SUMO) conjugation (SUMOylation) has been established as a form of posttranslational modification involved in the control of

88 intracellular protein stabilization, localization, and activity in plants and other
89 eukaryotes (Hay, 2005, 2013; Hendriks and Vertegaal, 2016; Vierstra, 2012). The
90 process of SUMOylation is facilitated by a series of enzymatic reactions that entail
91 SUMO activation, conjugation, and ligation, with these respective reactions being
92 catalyzed by SUMO-activating enzymes (E1), SUMO-conjugating enzymes (E2), and
93 SUMO ligases (E3) (Novatchkova et al., 2004). In systems focused on bacterial
94 reconstitution, E1 and E2 co-expression is sufficient to conjugate SUMO to most
95 substrates, providing a simplified system for the *in vitro* detection of SUMOylation
96 (Okada et al., 2009). The covalent SUMOylation of proteins is reversible through a
97 reaction catalyzed by sentrin-specific protease (SENP), which reportedly exhibits
98 nuclear localization (Li and Hochstrasser, 1999; Sun, 2008). SUMOylation, however,
99 can also affect proteins in the cytosol (Mabb et al., 2006), leading to the identification
100 in humans of members of the putative deubiquitinating isopeptidase PPPDE
101 superfamily of desumoylases designated DeSI-1/-2 (deSUMOylating isopeptidase 1/2)
102 (Shin et al., 2012). SUMO proteases identified to date in *Arabidopsis* have been
103 classified into the ubiquitin-like protease (ULP) and DeSI superfamilies, both of which
104 harbor a nucleophilic cysteine residue within the center of their catalytic site
105 dyads/triads that is required for the cleavage of the thioester bonds that form between
106 SUMO and target proteins (Morrell and Sadanandom, 2019). Eight predicted DeSI
107 proteases have been identified to date in *Arabidopsis* based on their similarity to human
108 DeSI1/2 sequences. Of these, Desi3a has been shown to play a functional role in plant
109 innate immunity (Orosa et al., 2018). In pepper, a study of the SUMOylation and

110 deSUMOylation of CaAITP1 has also established a role for CaDeSI2 in drought
111 responses and ABA signaling (Joo et al., 2024). However, a comprehensive
112 understanding of the DeSI2 proteins encoded in the maize genome, specifically,
113 whether they possess deSUMOylating activity, their roles in drought resistance, disease,
114 and quality improvement, and how they are regulated under biological conditions, is
115 lacking.

116 Here, the deSUMOylating isopeptidase gene *ZmDeSI2* was found to repress the
117 synthesis of Met through its ability to directly decrease the SUMOylation and protein-
118 level accumulation of ZmSIR, a sulfite reductase. ZmWRKY105 was further identified
119 as an upstream transcription factor involved in promoting the expression of *ZmDeSI2*
120 in inbred maize lines, demonstrating the value of ZmDeSI2 as a mediator of Met
121 biofortification in the breeding of nutrient-rich maize.

122 **Results**

123 **GWAS and transcriptomic-based identification of genes associated with**
124 **kernel Met content**

125 To identify genes related with Met content in maize kernels, a population of 348
126 historically utilized inbred lines from various heterotic groups was utilized, measuring
127 the kernel Met content from these inbred lines when grown in two consecutive years in
128 Changping and Gongzhuling County, China. The mean kernel Met content in this
129 population was 0.18%, with a range from 0.06-0.35% (Figure 1A, Supplemental Figure
130 1A-1C, Supplemental Figure 2). Based on these initial analyses of kernel protein
131 content phenotypes, 264 of these 348 inbred lines were resequenced as representative

132 materials with the aim of identifying the genomic basis for variably kernel Met content.
133 The resultant sequences were aligned to the B73 reference genome (Jiao et al., 2017),
134 leading to the identification of 11,929,554 single-nucleotide polymorphisms (SNPs)
135 with a minor allele frequency (MAF) exceeding 0.05 (Supplemental Figure 3,
136 Supplemental Table 1). These SNPs were leveraged to perform phylogenetic and
137 principal component analyses (PCA) of the representative germplasms for each
138 heterotic group, thereby enabling the quantification of relationships among these 264
139 lines and identifying five distinct groups, including PA (n=55), PB (n=54), Lancaster
140 (n=65), BSSS (n=58), and Tangsipingtou (n=32) (Figures 1B and 1C, Supplemental
141 Figure 4A). Linkage disequilibrium (LD) within each group declined with rising
142 physical distance between SNPs (Supplemental Figure 4B), with an average of 5 kb
143 (r^2=0.23).
144 To explore novel genes involved in the regulation of Met content within kernels, a
145 genome-wide association study (GWAS) of maize kernels was conducted, leading to
146 the identification of 211 significant loci associated with 193 genes based on phenotypic
147 data collected from individual environment and BLUE values (Figure 1D,
148 Supplemental Table 2, Supplemental Figures 5A-5C). A GWAS peak on chromosome
149 7 was consistent with the *zp27* quantitative trait locus (QTL) region (*Zm00001d020592*)
150 previously reported to encode the cysteine-rich 27-kDa *γ*-zein, which is a synthetic
151 precursor of Met precursor (Figure 1D).
152 To identify potential candidate genes, the Pearson correlation coefficients between gene
153 transcription and kernel Met levels in endosperm samples collected 20 days after

154 pollination, using transcriptomic sequencing to assess the levels of gene expression
155 (Chen et al., 2014) and yielding expression profiles for 46,430 genes across 348 inbred
156 lines. Of these genes, the expression levels of 93 were found to be significantly
157 correlated with kernel Met content (P<0.001), including *zp15*, *dzs18,* and *dzs10*, which
158 respectively encode 15-kDa β-zein, 18-kDa δ-zein, and 10-kDa δ-zein. These proteins
159 are rich in Cys and Met residues, respectively consisting of 15.63%, 26.84%, and 26.3%
160 Met + Cys residues (Supplemental Figure 6). The integration of these GWAS and
161 Pearson correlation analysis results led to the joint identification of *zp27* and
162 *Zm00001d002758* as the only relevant target locus (Figures 1E and 1F, Supplemental
163 Table 3). As annotations for *Zm00001d002758* indicated that it encodes a
164 deSUMOylating isopeptidase-like protein, it was designated as *ZmDeSI2*. Further
165 characterization of *ZmDeSI2* as a Met-related candidate gene led to the identification
166 of two *ZmDeSI2* haplotypes defined by non-synonymous SNPs. The kernel Met content
167 in *ZmDeSI2*^{Hap2} lines were found to be significantly higher than those of *ZmDeSI2*^{Hap1}
168 lines (P=5.74e-07), with a corresponding reduction in *ZmDeSI2* expression (P=1.05e-
169 50) (Figure 1G and 1H). *ZmDeSI2* may therefore function as a negative regulator of
170 kernel Met content. Cys was the synthetic precursor of Met, *ZmDeSI2* as a candidate
171 locus was not identified by GWAS on the Cys content in maize kernels (Supplemental
172 Figure 7A), and its haplotypes showed no significant associations with Cys
173 accumulation (P = 0.217) (Supplemental Figure 7B).

174 **ZmDeSI2 negatively regulates kernel Met content**

175 To examine whether *ZmDeSI2* could improve the Met content of maize kernels, an ethyl

176 methanesulfonate (EMS) mutant with prematurely terminated *ZmDeSI2* translation was
177 next obtained on the B73 background (Figures 2A-2C), and the mutant line presented
178 with an increase in kernel Met content in the BC_2F_2 and BC_3F_2 generations (Figure 2D).
179 An overexpression construct *pUbi:ZmDeSI2-Flag* was also introduced into the B73
180 inbred line, resulting in two independent transgenic events (Figure 2E). Compared to
181 B73, the T_2 transgenic lines exhibited significantly reduced kernel Met content (Figure
182 2F). To further confirm the functional role of *ZmDeSI2,* a CRISPR-Cas9 genome
183 editing approach was used to disrupt *ZmDeSI2* in B73, leading to the establishment of
184 two independent homozygous knockout (CR) transgenic lines. Both knockout lines
185 harbored *ZmDeSI2* frameshift mutations attributable to the deletion or insertion of bases
186 in exon regions (Figure 2G). These CR lines exhibited significant increases in kernel
187 Met content relative to B73 kernels ($P<0.0001$) (Figure 2I). However, no differences
188 in kernel length, kernel width, kernel thickness, hundred kernel weight, number of rows
189 per ear, or number of kernels per ear were observed when comparing the CR and wild-
190 type lines ($P>0.05$) (Figure 2H, 2J-2O). The knockout of *ZmDeSI2* thus increases
191 kernel Met content without any corresponding adverse effects on yield-related traits.

192 **ZmWRKY105 is a direct regulator of *ZmDeSI2* expression**

193 Given the observed negative correlation between *ZmDeSI2* expression and kernel Met
194 content in the inbred maize population (Figure 1E), the *ZmDeSI2* promoter and coding
195 regions from 10 high-Met and 10 low-Met maize lines harboring the $ZmDeSI2^{Hap1}$ or
196 $ZmDeSI2^{Hap2}$ haplotypes were cloned for analysis. Relative to $ZmDeSI2^{Hap1}$,
197 $ZmDeSI2^{Hap2}$ promoter was found to contain a 3416 bp deletion (Supplemental Figure

198 8A) with a 212 bp *Mu* transposon sequence (Supplemental Figure 9). *ZmDeSI2*^{Hap2}
199 simultaneously exhibited reduced *ZmDeSI2* expression and increased kernel Met
200 content relative to *ZmDeSI2*^{Hap1} lines (Supplemental Figures 8B-8D). To explore the
201 potential effects of natural variations beyond the promoter region on kernel Met content,
202 134 inbred lines were randomly selected from the inbred maize population for candidate
203 gene association analysis (Supplemental Table 4). While some of the individuals in the
204 *ZmDeSI2*^{Hap2} population additionally harbored a 1322 bp insertion in exon 2, variations
205 in the promoter regions emerged as the primary contributors to kernel Met content
206 (Supplemental Figure 8E). Furthermore, we demonstrated a significant association
207 between the presence or absence of specific promoter regions and kernel Met content
208 (r=0.41, P=6.51e-07). The active region of the promoter of ZmDeSI2^{Hap1} was analyzed
209 in *Nicotiana benthamiana* leaf-based transient dual-luciferase assays, showing that the
210 active region of the promoter was 250-1500 bp from the transcription initiation site.
211 (Figure 3A). In transient expression assays, the promoter activity of *ZmDeSI2*^{Hap1} was
212 significantly higher than that of *ZmDeSI2*^{Hap2} (P=1.15e-05) due to the loss of sequences
213 having highly active regions of transcription (Supplemental Figures 8F and 8G). These
214 results provide support for the impact of natural *ZmDeSI2* promoter variations on the
215 transcription of this gene.
216 *ZmDeSI2*^{Hap1} expression levels varied substantially and were associated with a
217 significant eQTL peak, suggesting that cis-acting elements or trans-acting factors
218 control the expression of this gene (Figure 3B). The integration of these predictive
219 transcription factor analyses and eQTL analysis results led to the joint identification of

220 eight transcription factors (Supplemental Table 5). A co-expression network was then
221 constructed to investigate the mechanisms controlling *ZmDeSI2* expression. This
222 showed that this gene was co-expressed with *Zmdzs10* (r=-0.22, *2.59*E-05)
223 (Supplemental Figure 10A). *Zmdzs10* encodes the 10- kDa δ-zein with the highest
224 content of Met, and its expression levels were found to be strongly correlated with
225 kernel Met content (r=0.46, P=1.42E-11) (Supplemental Table 3). Of the eight
226 transcription factors identified in predictive and eQTL analyses of *ZmDeSI2*
227 (Supplemental Table 5), only ZmWRKY105 (*Zm00001d004086*) was verified by the
228 eQTL results for *Zmdzs10* [(-log10(P)= 9.04] (Supplemental Figure 10B). Therefore,
229 we hypothesized that ZmWRKY105 may be a key transcription factor regulating both
230 the expression of *ZmDeSI2* and the kernel Met content.
231 To further probe the ability of ZmWRKY105 to regulate *ZmDeSI2*, analysis of the
232 *ZmDeSI2* promoter was conducted that detected a putative WRKY transcription factor
233 binding site comprised of GTCAA motif located 841 bp upstream of the transcriptional
234 start site (TSS). Due to the high degree of transcriptional activation by the promoter,
235 we divided the active region of the promoter (1500 bp from the transcription start site)
236 into 15 consecutive 100-bp fragments to eliminate background interference and enable
237 effective binding of ZmWRKY105 to the *ZmDeSI2* promoter. Yeast one-hybrid (Y1H)
238 assays and electrophoretic mobility shift assays (EMSAs) confirmed the ability of
239 ZmWRKY105 to bind this putative binding site, namely, the GTCAA motif with S9
240 (Figures 3C and 3D). In addition, new sites for WRKY105 binding were identified
241 through Y1H assays, EMSA, and CUT&Tag-qPCR, including S1, S3, S5, S10, S11,

242 S12, and S15 in the *ZmDeSI2* ^{Hap1} promoter (Figures 3C, 3E and 3F). In maize protoplast
243 and *Nicotiana benthamiana* leaf-based transient dual-luciferase assays, ZmWRKY105
244 was able to induce the expression of *ZmDeSI2*^{Hap1} but not *ZmDeSI2*^{Hap2} (Figures 3G-
245 3I). These findings indicate that ZmWRKY105 is a positive regulator of *ZmDeSI2*
246 expression that at least partially accounts for the differences in its expression among
247 maize haplotypes. To further clarify the genetic link between ZmWRKY105 and
248 *ZmDeSI2* in the context of the control of maize kernel Met content, and EMS mutant
249 exhibiting the premature termination of ZmWRKY105 translation was established on
250 the B73 background (Supplemental Figures 11A and 11B). In this *wrky105* line, the
251 significantly reduced *ZmDeSI2* expression (Figure 3J) and increased kernel Met content
252 (Figure 3K) is consistent with the status of ZmWRKY105 as an upstream inducer of
253 *ZmDeSI2* expression.

254 **ZmSIR is a ZmDeSI2 substrate protein**

255 The *ZmDeSI2* gene encodes a 209-amino-acid (aa) protein with a deSUMOylating
256 isopeptidase domain from amino acids 11 to 159 (Figure 4A). DeSI-2 is a
257 deSUMOylase in the PPPDE protein family that was first reported in humans. The
258 DeSI-2 cDNA sequence contains a 582 bp open reading frame (ORF) and encodes a
259 194-aa that shares 23% amino acid sequence identity with DeSI-1 (Figure 4B). The
260 presence of homologous genes in monocot and dicot species suggests that this gene
261 may be evolutionarily ancient in plants (Supplemental Figure 12A). Despite the
262 presence of a homologous gene, *Zm00001d026190*, in the maize genome that shared a
263 common domain with *ZmDeSI2* (Supplemental Table 6), no differences in Met content

264 were observed among the various haplotypes within the population (Supplemental
265 Table 7). This functional divergence likely resulted from evolutionary specialization
266 within gene families. Through gene expression analyses, the preferential expression of
267 *ZmDeSI2* was noted in stems and endosperms at 20 days after pollination (DAP)
268 (Supplemental Figure 12B).

269 In subcellular localization analyses, ZmDeSI2 was found to localize to both the cytosol
270 and cell membrane, mirroring the localization pattern of DeSI-2 (Figure 4C,
271 Supplemental Figure 12C). A luciferase complementation imaging (LCI) assay was
272 next used to screen for substrates modified by ZmDeSI2 related to Met biosynthesis
273 localized to the cytosol, including key Met metabolism pathway-related enzymes and
274 the products of Met-rich zein synthesis genes (*zp15* and *dzs10*) (Supplemental Figure
275 12D). This approach revealed the ability of ZmDeSI2 to interact with Zmdzs10,
276 ZmCGS1, ZmCGS2, ZmCBL, and ZmSIR associated with the positive regulation of
277 Met synthesis (Figure 4D). We used the overexpression material of *ubi:ZmDeSI2-Flag*
278 for immunoprecipitation-mass spectrometry (IP-MS) analysis, finding significant
279 enrichment of ZmSIR protein levels (Supplemental Table 8). In addition, ZmSIR is the
280 only major gene in which natural variants have been found to affect Met content (Jiang
281 et al., 2021). Bimolecular fluorescence complementation (BiFC) assays performed in
282 *N. benthamiana* leaves further confirmed the ability of ZmDeSI2 and ZmSIR to interact
283 *in vivo* (Figures 4E and 4F). Consistently, Flag-ZmDeSI2 expressed in *E. coli* strain
284 BL21 (DE3) was successfully pulled down *in vitro* by His-ZmSIR but not by His alone
285 (Figure 4G). ZmDeSI2 and ZmSIR therefore directly interact with one another *in vitro*

286 and *in vivo.*

287 To assess the potential SUMOylation of ZmSIR, LCI and BiFC assays were used to test
288 for ZmSIR interactions with the E2 SUMO-conjugating enzyme when transiently
289 expressed in *N. benthamiana* leaves. This ZmSIR-E2 interaction was confirmed in these
290 assays (Figures 4H and 4I), and was also independently validated through *in vitro*
291 assays in which His-ZmSIR but not His alone was able to facilitate the pull-down of E2
292 (Figure 4J). ZmSIR was also found to interact directly with ZmSUMO1a (Supplemental
293 Figures 13A-13D). GPS-SUMO predictions also identified the presence of a putative
294 SUMOylation site on ZmSIR (Supplemental Figure 14A). In LCI and BiFC assays, E2
295 was able to interact with ZmSIR but not with the ZmSIR-T variant lacking this
296 predicted SUMOylation site (Supplemental Figures 14B-14E). Based on these results,
297 ZmSIR can undergo SUMOylation both *in vitro* and *in vivo.*

298 **ZmDeSI2 functions as a deSUMOylase that reduces ZmSIR protein stability**

299 While the presence of a protease domain led to the prediction that ZmDeSI2 functions
300 as a deSUMOylating peptidase, no corresponding experimental validation of this
301 deSUMOylating activity has yet been performed. The potential deSUMOylating
302 activity of ZmDeSI2 was initially analyzed *in vitro* by coexpressing appropriate
303 combinations of E1, E2, ZmSUMO1a, ZmSIR, and ZmDeSI2 in *E. coli* BL21 (DE3)
304 cells, followed by evaluation of the ZmSIR SUMOylation status. In these experiments,
305 the amount of ZmDeSI2 protein added was found to be associated with a decrease in
306 SUMOylated ZmSIR levels (Figure 5A). Accordingly, *in vivo* analyses were performed
307 in *N. benthamiana* through the co-expression of *35S:ZmSIR-Flag* with *35S:Myc*,

308 *35S:ZmSIR-Flag* with *35S:ZmSUMO1a-Myc*, *35S:ZmSIR-Flag* and *35S:ZmSUMO1a-*
309 *Myc* with *35S:ZmDeSI2-His, 35S:Myc* with *35S: ZmSIR-T-Flag* which has mutated
310 sequences at SUMOylation sites and *35S:ZmSUMO1a-Myc* with *35S:ZmSIR-T-Flag*.
311 Immunoblotting analyses of ZmSIR SUMOylation status in these samples revealed that
312 ZmSIR can be modified by SUMOylation, and mutations at the SUMOylation sites of
313 ZmSIR, along with the overexpression of ZmDeSI2, can lead to a pronounced decrease
314 in SUMOylation-modified ZmSIR levels (Figure 5B).
315 To further verify the influence of ZmDeSI2 on ZmSIR protein accumulation *in vivo*,
316 western blotting was used to measure ZmSIR protein levels in B73, *desi2* mutants, and
317 ZmDeSI2-OE transgenic lines using anti-ZmSIR antibodies. The results showed a
318 marked increase in ZmSIR protein levels in the *desi2* mutants together with clear
319 reductions in the ZmDeSI2-OE lines compared to B73 (Figure 5C). We also clarified
320 the ability of ZmDeSI2 to affect the *in vivo* accumulation of ZmSIR at the protein level
321 in *N. benthamiana* leaves through co-expression of the different constructs, and ZmSIR
322 protein levels were detected by immunoblotting in a protein degradation assay
323 performed. In this assay, ZmSUMO1a-Myc was able to significantly suppress ZmSIR-
324 Flag degradation relative to empty Myc (EV) vector, while the presence of ZmDeSI2-
325 His was associated with the enhancement of such degradation relative to the co-
326 expression of ZmSUMO1a-Myc and ZmSIR-Flag/ZmSIR-T-Flag. The stability of the
327 ZmSIR-T protein decreased after mutation of the SUMOylation site, consistent with the
328 observed effect in ZmDeSI2-overexpressing plants (Figure 5D and 5F). The
329 proteasome inhibitor MG132 was also able to suppress ZmSIR-Myc degradation

330 (Figures 5E and 5G). Together, these results demonstrate that SUMOylation can reduce
331 the degradation of ZmSIR, whereas this inhibitory effect is counteracted by ZmDeSI2-
332 mediated deSUMOylation through a mechanism that may involve 26S proteasome-
333 mediated degradation.

334 In cell-free degradation assays, immunoblotting analyses of ZmSIR-His levels revealed
335 a marked decrease in the rate of ZmSIR-His degradation in *desi2* extracts relative to
336 those from B73 (Figures 5H and 5J). Furthermore, overexpression of ZmDeSI2,
337 enhanced the degradation of ZmSIR (Figures 5L and 5N). The proteasome inhibitor
338 MG132 was also able to prevent this ZmSIR-His degradation for both WT, *desi2* mutant
339 and ZmDeSI2-OE extracts (Figures 5I, 5K, 5M, and 5O). These data demonstrate the
340 ability of the deSUMOylase activity of ZmDeSI2 to reduce the stability of ZmSIR *in*
341 *vitro* and *in vivo* through the removal of the SUMO modification from this protein,
342 rendering it more sensitive to proteasomal degradation.

343 To determine Met levels in the hypothetical double mutants of *zmdesi2* and *zmsir*, we
344 analyzed the *ZmSIR* haplotypes in the inbred maize population. *ZmSIR* was found to
345 exist in two haplotypes, with $ZmSIR^{Hap1}$ showing higher Met content than $ZmSIR^{Hap2}$. It
346 was considered that $ZmSIR^{Hap1}$ should be the functional genotype (Supplemental Figure
347 15A). In the $ZmSIR^{Hap1}$, by comparing the mutated $ZmDeSI2^{Hap2}$ with the functional
348 $ZmDeSI2^{Hap1}$, it was found that the mutant phenotype of $ZmDeSI2^{Hap2}$ exhibited
349 significantly higher Met content than the phenotype with normal $ZmDeSI2^{Hap1}$
350 expression. In $ZmSIR^{Hap2}$ (9 lines), we analyzed the *ZmDeSI2* genotypes and found that
351 when both $ZmDeSI2^{Hap1}$ and $ZmSIR^{Hap2}$ carried non-elite haplotypes, the kernel Met

content was minimal. The *ZmDeSI2*^{Hap2} functional mutation thus partially rescued the *ZmSIR*^{Hap2} phenotype (Supplemental Figures 15B and 15C). It was suggested that the absence of deSUMOylation in ZmSIR enhanced its accumulation and increased both the stability and accumulation of the protein.

Marker–assisted selection of maize varieties with Met-enriched kernels

To systematically explore variations in kernel Met content in the context of maize breeding, kernel Met content BLUE values were next compared across five heterotic groups. On average, significantly higher Met content levels were observed in the PA group relative to the other groups (Figure 6A). The potential selection of *ZmDeSI2* over the course of maize breeding was analyzed by investigating *ZmDeSI2*^{Hap2} frequencies in variant groups. Over 87.5% of inbred lines were found to be carriers of the elite *ZmDeSI2*^{Hap2} haplotype in the PA group, as compared to just 33.3% of the inbred lines in the PB group. This supports the status of *ZmDeSI2* as a major genetic determinant of the increased kernel Met content in germplasms in the PA group (Figure 6B). However, no noticeable variations in kernel Met content were observed when comparing three different breeding generations, namely, 1980&90s, 2000s, and 2010s ($P \geqslant 0.15$) (Supplemental Figure 16). Fixation index (Fst) and composite likelihood ratio (XP-CLR) analyses provided further support for *ZmDeSI2* selection when comparing the PA and PB groups (Figures 6C and 6D). Based on these results, *ZmDeSI2*^{Hap2} appears to hold promise as a target for modern maize breeding efforts.

To aid in the selection of maize varieties with Met-enriched kernels, the 3416-bp presence-absence variation (PAV) that differs between the *ZmDeSI2*^{Hap1} and

374 *ZmDeSI2*^{Hap2} promoter regions was next tested as a potential molecular marker for Met
375 biofortification (Figure 6E). Marker validation was achieved by selecting 40 inbred
376 lines that had not undergone resequencing data-based classification as a test population.
377 Those inbred lines carrying *ZmDeSI2*^{Hap2} exhibited reduced *ZmDeSI2* expression
378 together with higher levels of Met content (P<0.001) (Figures 6F and 6G), confirming
379 the performance of this marker. *ZmDeSI2*^{Hap2} was subsequently introduced into the
380 WC009 line from the PB group with low Met content through a marker-assisted
381 selection approach. This WC009 line was derived from the Zheng 58/Mo17 basic
382 material selection population and is the male parent of the commercially successful
383 hybrid Heyu187 maize variety. Relative to parental WC009, the developed homozygous
384 near-isogenic lines (WC009^{NILs}) presented the significantly reduced *ZmDeSI2*
385 expression with significant increases in kernel Met content (Figures 6I and 6J). In
386 contrast, no differences in kernel length, kernel width, kernel thickness, hundred kernel
387 weight, number of rows per ear, and number of kernels per row were observed when
388 comparing the WC009^{NILs} and WC009 (P>0.05) (Figures 6H, 6K-6P). These data
389 underscore the value of the natural *ZmDeSI2*^{Hap2} variant as a valuable genetic resource
390 for the Met biofortification of maize crops without any reduction in yield.

391 **Discussion**

392 Despite being the second most limiting amino acid in maize, the process of Met
393 biosynthesis in this important crop species is far less well understood as compared to
394 its elucidation in *Arabidopsis* (Leustek, 2002). As animals are unable to assimilate
395 sulfate, they are dependent on dietary sulfur-containing proteins and amino acids,

396 emphasizing the important status of plants in the global sulfur cycle (Maruyama-
397 Nakashita, 2017). Each ton of full-priced feed generally contains 1-2 kg of
398 supplemental Met. At current global average Met prices of 3.0 USD/kg, approximately
399 1.3 million tons of Met are added to livestock feed annually. A 0.1% increase in the Met
400 content in maize has the potential to reduce global annual feed costs by at least 39
401 billion USD (https://www.feedinfo.com/). Met is also a key amino acid for all living
402 organisms, supporting the formation of proteins, enzymatic cofactors, lipids,
403 polysaccharides, and iron-sulfur clusters (Koprivova and Kopriva, 2016). In the context
404 of crop production, Met and sulfur deficiencies have increasingly emerged as a topic of
405 concern over recent decades in Asia, Europe, and the Americas (Jackson et al., 2015),
406 given that prolonged sulfur depletion can result in severely stunted growth, impaired
407 biotic stress resistance, and substantial yield losses (Armbruster et al., 2019). While
408 heterologous Met assimilation pathway synthase gene expression can improve Met
409 levels in maize germplasms (Planta et al., 2017; Xiang et al., 2018; Yang et al., 2018),
410 persistent biosafety concerns limit the application of this approach in maize breeding
411 programs. It is thus vital that naturally Met-rich maize germplasm resources be
412 identified.

413 Recent advances in GWAS and QTL mapping approaches have enabled the discovery
414 of many genetic variants that account for the phenotypic differences observed when
415 comparing teosinte and maize (Guo et al., 2018; Huang et al., 2022; Tian et al.,
416 2019), or when exploring the variations evident among maize accessions (Huang et al.,
417 2022; Li et al., 2022; Li et al., 2023a; Li et al., 2013; Wang et al., 2020; Wang et al.,

418 2016). QTLs are involved in the regulation of amino acid levels in plants, with several
419 loci having been linked to the levels of sulfur-rich amino acids in soybeans (Deng et al.,
420 2017; Jiang et al., 2021; Panthee et al., 2006; Wang et al., 2015). Studies aimed at
421 producing maize varieties with high-quality protein content have focused primarily on
422 efforts to increase the lysine content. While this has led to the successful identification
423 of several lysine-rich mutants, including *o2*, *floury2*, and *opaque7*, there have been no
424 similar successes in the production of varieties with enhanced kernel Met content
425 (Mertz et al., 1964; Nelson et al., 1965). To date, however, there have been few studies
426 aimed at clarifying the genetic regulation of sulfur-rich amino acid accumulation in
427 maize. The advent of multi-omics and systems biology techniques and technologies has
428 improved the feasibility of conducting research focused on material differences at the
429 genomic, transcriptional, translational, and metabolic levels. These strategies can yield
430 more comprehensive insights into the genetic mechanisms and metabolic pathways that
431 underlie complex quantitative trait emergence in crops (Li et al., 2013; Li et al., 2023b;
432 Ma et al., 2021; Sang and Kong, 2024; Tang et al., 2021; Zhang et al., 2022). Even with
433 these advances, natural variation applicable to the breeding of biofortified varieties
434 remains limited (Deng et al., 2017). In this study, integrated GWAS, correlation, and
435 eQTL mapping analyses were used to identify *ZmDeSI2*, an uncharacterized
436 deSUMOylating isopeptidase, in the maize genome (Figures 1D and 1E, Figure 3A).
437 These analyses offer unprecedented insight into the molecular processes that control
438 maize Met biosynthesis, and led to the identification of a previously unrecognized elite
439 natural allelic variant suitable for use in the breeding of Met-enriched maize varieties.

440 Transposon-based insertion in or near specific genes is the most common source of
441 distinct genomic variations, as these transposons can interfere with gene transcription
442 at the genetic or epigenetic levels (Mao et al., 2015; Yang et al., 2013; Zhang et al.,
443 2018). The maize genome harbors many transposable elements, many of which exhibit
444 relatively high levels of activity and are relevant to the evolution of this crop species
445 (Su et al., 2019; Zhang et al., 2014). Transposon-derived variants most commonly
446 repress transcriptional activity, raising the question of how alleles that increase
447 transcriptional activity may be favored in the context of natural selection (Mao et al.,
448 2015; Yang et al., 2013). Relative to *ZmDeSI2*^{Hap1}, *ZmDeSI2*^{Hap2} was found to exhibit
449 significantly reduced transcriptional activity due to the deletion of a
450 substantial sequence from the promoter region. The *ZmDeSI2*^{Hap1} promoter contains a
451 212 bp *Mu* transposon sequence, which may have contributed to this loss of a large
452 amount of genomic material from the *ZmDeSI2*^{Hap2} promoter. Multi-omics strategies are
453 often leveraged for the purposes of QTL identification and co-expression network
454 construction, but the validation of associated regulatory mechanisms is not routinely
455 performed (Deng et al., 2017; Li et al., 2013; Li et al., 2023b; Ma et al., 2021; Zhang et
456 al., 2022). Here, ZmbZIP22 was found to regulate the transcription of *ZmDeSI2*^{Hap1}
457 (Supplemental Figures 17A and 17B). ZmbZIP22 can directly bind to the ACAGCTCA
458 box in the 27-kD *γ*-zein promoter and is also capable of interacting with PBF1, OHP1,
459 and OHP2, but not with O2 (Li et al., 2018a). Reductions in Met content observed
460 following the mutation of ZmbZIP22 are consistent with the phenotypes exhibited by
461 ZmDeSI2 mutants, providing further support for the ability of ZmbZIP22 to promote

462 *ZmDeSI2* expression[58]. ZmWRKY105 a member of the WRKY transcription factor that
463 are often associated with abiotic and biotic stress responses (Goyal et al., 2023; Jiang
464 et al., 2017; Rushton et al., 2012; Wang et al., 2018a), but there has been little research
465 implicating WRKY proteins in the synthesis of amino acids. Here, analyses of
466 ZmWRKY105 as an upstream regulator of *ZmDeSI2* transcription aided in the
467 identification of polymorphisms important for the transcription of this gene, enabling
468 the construction of a more comprehensive regulatory network. ZmDeSI2 is a protein in
469 the PPPDE family that is predicted to serve as a deSUMOylating peptidase owing to
470 the presence of a protease domain in some members of this family(Shin et al., 2012).
471 This study is the first to have directly demonstrated the deSUMOylating activity of
472 ZmDeSI2. Together, the present findings provide new insights into the molecular
473 mechanisms that govern the biosynthesis of Met (Figure 7).
474 Population material composition accounts for the origins of elite alleles. While some
475 QTLs have been cloned to date, the corresponding elite alleles have only rarely been
476 leveraged in the context of temperate breeding (Deng et al., 2017). Here, an elite
477 haplotype of *ZmDeSI2* affecting kernel Met was identified through a GWAS approach
478 based on inbred commercial germplasm resources planted over multiple years. After
479 identifying the elite natural *ZmDeSI2*^{Hap2} variant, it was introduced into the WC009
480 variety, leading to a 1.36-fold increase in kernel Met content. These results thus provide
481 a valuable resource for Met biofortification-focused maize breeding efforts. Met
482 content in PA and BSSS, belonging to Reid germplasms, were also significantly higher
483 than those of the non-Reid PB and Lancaster germplasms. The Reid germplasm

484 BSSS53 has long been leveraged as a donor when seeking to improve maize Met
485 content (Olsen et al., 2003). Near-complete *ZmDeSI2*^{Hap2} fixation was evident in the PA
486 group whereas it was largely absent from the PB group among the 264 analyzed
487 accessions. The elite *ZmDeSI2*^{Hap2} lines can thus serve as donors to improve kernel Met
488 content in maize germplasms in the PB group. There have been pronounced efforts on
489 behalf of maize breeders to improve the nutritional quality of maize for humans and
490 livestock. In one prior report, the natural selection of a subset of sulfur-rich zeins was
491 observed over the course of maize domestication (Li et al., 2018b). However, no
492 noticeable variations in kernel Met content were observed when comparing three
493 different breeding generations: 1980&90s, 2000s, and 2010s ($P \geqslant 0.15$). As an
494 apparently invisible trait, selection on *ZmDeSI2,* together with ZmSIR, may have
495 supported the adaptation of maize to high-altitude regions, potentially through
496 beneficial effects on abiotic stress resistance or nutritional biofortification (Jiang et al.,
497 2021; Orosa et al., 2018). Global climate change has intensified environmental stressors,
498 such as drought, flooding, extreme temperatures, salinity, and alkalinity, adversely
499 affecting crop growth and food yield and thereby threatening the sustainability of the
500 food supply (Yang et al., 2023). Given that *CaDeSI2* has been reported to participate in
501 drought tolerance in pepper (Joo et al., 2024) and that elevated Met levels can also
502 contribute to enhanced salt tolerance (Shi et al., 2025), it is therefore highly likely that
503 lines carrying improved alleles of *ZmDeSI2* can simultaneously enhance both kernel
504 quality and stress resilience. Moreover, the population used in the present study
505 comprises parental lines that have been selected for many years, with the retention of

506 favorable alleles during the breeding process, especially within the PA subgroup, where
507 accumulation has occurred. The improved ZmDeSI2^{Hap2} lines, therefore, represent
508 valuable genetic resources for the breeding of maize varieties that exhibit both superior
509 quality and enhanced abiotic stress tolerance.

510 In conclusion, these results support a model (Figure 7) in which *ZmDeSI2* haplotypes
511 divergently control the Met content in maize kernels. The loss-of-function *ZmDeSI2*^{Hap2}
512 may provide a resource for the breeding of maize varieties with improved kernel Met
513 content. In addition to providing insight into the molecular mechanisms that govern
514 maize Met biosynthesis, these findings thus provide a foundation for the development
515 of maize lines with improved nutritional properties.

516 **Materials and methods**

517 **Plant materials and phenotypic measurements.** The 348 elite inbred lines used to
518 conduct this study were selected from publicly available pedigrees, hybrid registrations,
519 and through personal communications with maize breeders. From among these inbred
520 lines, 264 representative germplasms were selected to establish a kernel protein
521 phenotype-focused GWAS panel. Of these accessions, 151 had known genotypes, while
522 the remaining 113 were subjected to whole-genome sequencing and aligned with the
523 B73 reference genome (B73_V4, ftp://ftp.ensemblgenomes.org/pub/plants/release-
524 37/fasta/zea_mays/dna) (Jiao et al., 2017), achieving an average coverage depth of
525 29.80 for each accession. For phenotypic analyses, these inbred lines were planted in
526 three environments over two consecutive years, including Changping, Beijing, China,
527 in 2018 (2018CP) and 2019 (2019CP), as well as in Gongzhuling County, Jilin Province,

528 China, in 2018 (2018GZL). All trials employed a randomized complete block design
529 using three replicates, with respective row and column spacings of 0.60 and 0.25 m.
530 Phenotyping analyses were performed for a minimum of five plants from the middle of
531 each plot. WC009 is the parent of Heyu187, a hybrid variety cultivated extensively
532 throughout northern China that carries the *ZmDeSI2*^{Hap1} haplotype. WC009 was used
533 for the validation of the improved parental line derived from the elite *ZmDeSI2*^{Hap2}
534 natural variant. EMS mutants resulting in the premature termination of the translation
535 of *ZmDeSI2* and ZmWRKY105 on the B73 background were obtained from the EMS
536 mutant library (memd,http://elabcaas.cn/memd/public/). These EMS mutants were
537 homozygous at the *ZmDeSI2* and *ZmWRKY105* loci. Then *desi2* was backcrossed with
538 B73 to generate BC_2F_2 and BC_3F_2 lines to use for phenotypic analyses while
539 minimizing any potential off-target effects.

540 **Amino acid analyses.** The levels of 17 different amino acids in the kernels of mature
541 inbred lines were quantified with an automated amino acid analyzer (L-8900, Hitachi
542 Instruments Engineering, Tokyo, Japan). Briefly, 100 mg of kernel powder per sample
543 was dissolved for 22 h in 10 mL of 6 M HCl at 110°C, followed by the filtration-based
544 removal of insoluble material and the transfer of these samples into 100-mL volumetric
545 flasks. Deionized water was then added to a final volume of 100 mL, samples were
546 mixed thoroughly, and 1 mL of the resultant solution was transferred into a 2 mL tube
547 and injected into the amino acid analyzer, using the L-8900 software ASM to analyze
548 the resultant raw data (Zhou et al., 2009).

549 **Estimating breeding value.** The breeding values of kernel Met content traits across all

trials were estimated in *R* with a linear mixed model using the *lme4* package(Bates et al., 2015):

$Y_{ij} = \mu + Line_i + Env_j + (Line \times Env)_{ij} + Env \times Rep_{jn} + error_{ijn}$

Where μ denotes the mean, $Line_i$ corresponds to the genotype effect of the *i*-th inbred, Env_j is the effect of the *j*-th environment, $(Line \times Env)_{ij}$ indicates the genotype-environment interaction, and $(Env \times Rep)_{jn}$ represents the environment-replication interaction. The $error_{ijn}$ error term accounts for the *j*-th environment and the *n*-th replicate of the *i*-th inbred, setting all items to random effects. Multiple comparisons testing for trait values were performed with the least significant difference (LSD) method in the R *agricolae* package (https://cran.r-project.org/web/packages/agricolae/). A Bonferroni-corrected $P < 0.05$ was considered significant.

Resequencing, mapping, and variant calling. DNA-seq libraries for each of the 264 inbred lines were prepared as directed by the manufacturer (Illumina Inc., San Diego, CA, USA), after which 150 bp paired-end sequencing was performed with the NovaSeq X system. Both the resequencing reads for the 113 inbred lines sequences in the present study and the corresponding sequence data for the 151 inbred lines published previously were mapped to the B73 genome (B73_V4, ftp://ftp.ensemblgenomes.org/pub/plants/release-37/fasta/zea_mays/dna) (Jiao et al., 2017) using the BWA (v.0.7.17-r1188) software with default parameters. SNPs and InDel calling were independently performed with GATK (ver. 3.1.1) and SAMtools (ver. 0.1.19) (Li and Durbin, 2009), retaining those sites identified using both of these methods. Variants were filtered based on the lack of the variant in ⩾10% of samples,

572 a minor allele frequency (MAF)≤ 0.05, and a heterozygosity rate ≥20%, yielding
573 11,929,554 biallelic SNPs for GWAS analyses. The annotation of genomic variants was
574 performed with the ANNOVAR package based on the B73 reference genome (Wang et
575 al., 2010). In total, 821,913 and 9,850,822 SNPs were respectively identified in genic
576 and intergenic regions. The ratio of nonsynonymous to synonymous substitutions in
577 coding regions was 1.6% (Supplemental Table 1, Supplemental Figure2), consistent
578 with what has been reported previously for a population of elite inbred lines (Chia et
579 al., 2012; Jiao et al., 2012; Wang et al., 2020).

580 **Population genetic analysis.** Phylogenetic analyses were performed by filtering out
581 variants when the variant was absent in ≥10% of samples, the MAF was ≤0.05, and
582 the heterozygosity rate was ≥0%, yielding 1,690,640 biallelic SNPs. A principal
583 component analysis (PCA) was conducted with Eigensoft (Price et al., 2006) based on
584 76,551 exonic SNPs. The population structure of these inbred lines was then
585 represented by the first three principal components (PC1: 7.48%, PC2: 4.21%, PC3:
586 3.84%), which collectively explained 15.53% of the observed genotypic variation. The
587 ADMIXTURE tool was then used to conduct a model-based analysis aimed at
588 validating these results (Alexander et al., 2009), using a five-fold cross-validation
589 approach to determine the number of ancestral populations (K) for these inbred lines in
590 this tool. At K = 5, the sharp convergence of cross-validation error was observed,
591 consistent with this being a reasonable estimate for the ancestry of these inbred lines.
592 Based on this selected value (K = 5), inbred lines were categorized into five groups
593 (SPT, PA, BSSS, PB, and LAN). The representative inbred lines for the SPT, PA, BSSS,

594 PB, and LAN groups were Huangzaosi, Zheng 58, B73, PH4CV, and Mo17.

595 **LD analysis.** Linkage disequilibrium (LD) analyses were performed for each
596 subpopulation based on SNPs with a MAF > 0.05. The LD for these 264 inbred lines
597 was estimated by using the PopLDdecay software to compute the average squared
598 correlation coefficient (r^2) between pairwise SNPs within 1000-kb windows using the
599 following parameters: -MaxDist 1000 -MAF 0.05 -Miss 0.1. The overall LD decay
600 distance among these 264 inbred lines was calculated at 5 kb ($r^2 = 0.23$) (Purcell et al.,
601 2007).

602 **GWAS for kernel Met content.** To conduct a GWAS analysis focused on kernel Met
603 content, 11,929,554 high-quality SNPs (MAF>0.05) from 264 inbred lines were utilized.
604 A mixed linear model (MLM) was used to perform association analyses in the Efficient
605 Mixed-Model Association expedited (EMMAX) software (Kang et al., 2010). These
606 SNPs were used to calculate kinship. The genome-wide significance cutoff for these
607 analyses was 1×10^{-5} (Benjamini–Hochberg false discovery rate [FDR]<0.05). For
608 adjacent GWAS loci, genes within a distance of up to 20 kb were considered
609 independent if they exhibited an $r^2<0.5$ in pairwise SNP linkage analyses. Candidate
610 genes for GWAS loci were identified based on genes present within a maximum of 5
611 kb of the confidence interval (genome-wide average distance of LD decay to $r^2 = 0.23$).

612 **Correlation analyses.** A population of 348 inbred maize lines was used to analyze
613 correlations between normalized expression values and phenotypic data. Normalized
614 expression data were generated through 150-bp paired-end RNA-sequencing analyses
615 of kernels collected 20 days DAP on an Illumina instrument, generating an average of

616 7.7 Gb of high-quality raw data from each of these inbred lines. Phenotypic data for
617 these inbred lines were collected after their planting in Gongzhuling and Changping in
618 2018 and 2019 as described above. Five ears per block were self-pollinated, and RNA-
619 seq analyses were performed using 20 immature endosperms from two ears per block
620 collected at 20 DAP in Changping in 2019. As correlations in kernel Met content were
621 observed across these three planting environments, subsequent analyses were
622 performed with Best Linear Unbiased Estimate (BLUE) values (r>0.74, P<0.001)
623 (Supplemental Figure 2). Correlations between phenotypic BLUE values and gene
624 expression levels were assessed based on correlation coefficients and P-values in the
625 *Corrplot* package in *R*. The filtered maize gene list was obtained from MaizeGDB
626 (http://www.maizegdb.org) to facilitate the identification of candidate genes within
627 quantitative trait loci (QTL).

628 **Plasmid construction and plant transformation**

629 Inbred B73 and *ZmDeSI2* knockout maize lines were obtained from Weimi Biotech Co.,
630 Ltd. The target sequences selected for this gene are presented in Figure 2E. The
631 *ZmDeSI2* target regions were amplified from B73 together with the corresponding
632 transgenic lines, followed by sequencing-based identification of the corresponding
633 mutations in these regions. Two independent homozygous *ZmDeSI2* knockout lines
634 were ultimately obtained that were designated CR-1 and CR-2. The coding sequences
635 of ZmDeSI2 were also amplified and inserted into the NEWMOL-3×Flag vector to
636 generate the constructs *pUbi:ZmDeSI2-Flag* in the B73 recipient line, resulting in two
637 independent transgenic events. The phenotypic characteristics of these transgenic

638 events and wild-type B73 were analyzed under normal field planting conditions in
639 Changping, Beijing, China in 2023. Replicate mutant and neighboring wild-type control
640 plots were established (row spacing: 0.60 m, column spacing: 0.25 m), with two
641 replicates for these phenotyping trials.

642 **eQTL mapping.** Expression quantitative trait locus (eQTL) analyses examining the
643 relationship between SNPs and gene expression were performed using the GWAS
644 approach described above. Briefly, association analyses were performed to explore the
645 association between genome-wide SNPs and candidate gene expression levels, only
646 analyzing those genes expressed in >50% of the 264 inbred lines with at least 10
647 available reads (Liu et al., 2016).

648 **Yeast one-hybrid (Y1H) assays.** Y1H assays were performed as in a prior report (Lin
649 et al., 2007). To produce the pB42AD-ZmWRKY105 prey vector, the *ZmWRKY105*
650 coding sequence (CDS) was introduced into the pB42AD vector at the *EcoR*I restriction
651 site, while the pLacZi-*ZmDeSI2* bait vector was generated by cloning the *ZmDeSI2*
652 promoter sequence into the pLacZi reporter vector at the *Xho*I restriction site. The
653 EGY48 yeast strain was then co-transformed with these bait and prey vectors, followed
654 by the culture of transformants for 3 days on SD-Trp/-Ura plates at 28°C, after which
655 galactosidase activity was analyzed by transferring them onto X-Gal (5-bromo-4-
656 chloro-3-indolyl-*β*-D-galactopyranoside) plates. As negative controls, EGY48 co-
657 transformation was performed using the empty pB42AD or pLacZi vectors in
658 combination with pLacZi-*ZmDeSI2* or pB42AD-ZmWRKY105.

659 **Electrophoretic mobility shift assay (EMSA).** A ZmWRKY105-GST fusion protein

660 was prepared by ligating the *ZmWRKY105* CDS into the pET30a vector (Cat#ZK132,
661 ZOMANBIO, Beijing) and using this construct to transform the *E. coli* BL21 (DE3)
662 strain. ZmWRKY105-GST expression was induced by adding 0.2 mM isopropyl-*β*-D-
663 thiogalactopyranoside (IPTG) to these *E. coli* cells in LB broth or 12 h at 15°C. GST
664 fusion protein magnetic beads (Cat#M2320, Solarbio, Beijing) were used as directed in
665 the provided manual (http://www.novagen.com) to purify ZmWRKY105-GST and the
666 control pGEX4T-1 protein. The fused protein was eluted with 20 mM Tris–HCl at pH
667 8.0 containing 10 mM glutathione. A double-stranded *ZmDeSI2* probe used for these
668 experiments was the same as that used for DNA pull-down. Both the *ZmDeSI2* probe
669 and the ZmWRKY105-GST fusion protein were combined with 20 μL of binding buffer
670 [100 mM Tris, 500 mM KCl, 10 mM DTT, 2.5% glycerol, 0.2 mM EDTA, 50 ng/μL
671 poly(dI–dC)] for 25 min at room temperature, followed by the separation of samples
672 with 4 μL of 5× protein loading buffer (1 M Tris–HCl, 10% sodium dodecyl sulfate, 25
673 mg bromophenol blue, 250 μL of *β*-mercaptoethanol) using 8% native polyacrylamide
674 gels and subsequent transfer to a nylon membrane. Biotin-labeled DNA probes were
675 then detected with a LightShift Chemiluminescent EMSA Kit (Cat#20148, Thermo
676 Fisher Scientific) as directed.

677 **Nucleus CUT&Tag-qPCR.** *ZmDeSI2-GFP*-overexpressing nodules were collected for
678 modified nCUT&Tag-qPCR. Fresh nodules (0.2 g) were homogenized in PBS
679 containing protease inhibitors, filtered through 40-μm cell strainer to isolate the plant
680 nuclei. After centrifugation (12000 g, 5 min) and washing with PBS, the nuclei were
681 stained with DAPI for microscopic verification. Subsequent CUT&Tag steps involved

682 binding to ConA beads, sequential incubation with anti-GFP primary (Abcam, ab31629)
683 and secondary antibodies (Abcam, ab6701), followed by pA/G-transposome assembly
684 and tagmentation. The DNA libraries were amplified after proteinase K digestion, with
685 no-primary-antibody controls (Hieff NGS Tagment Index Kit for Illumina ®,
686 12416ES24). The qPCR reactions utilized SYBR-based detection (Tiangen Biotech Co.
687 Ltd., China) using the cycling parameters of 95°C/15 min, followed by 40 cycles of
688 95°C/10 s-58°C/20 s-72°C/20 s. All experiements included three technical replicates.

689 **Transient dual luciferase (dual-LUC) assay.** The pro*ZmDeSI2*^{Hap1}-LUC and
690 pro*ZmDeSI2*^{Hap2}-LUC reporter constructs were prepared by amplifying the
691 *ZmDeSI2*^{Hap1} and *ZmDeSI2*^{Hap2} promoter sequences from B73 and HP434, respectively,
692 and introducing them into the pGreenII 0800-LUC vector. Maize protoplasts and *N.*
693 *benthamiana* leaves were then used for transient transactivation assays, using the
694 pro*ZmDeSI2*^{Hap1}-LUC constructs served as reporters and the ZmWARY105 constructs
695 were cloned into the transient expression vector *35S:*ZmWARY105-*GFP*, acting as
696 effectors. The approach enabled the testing of the ability of ZmWARY105 to regulate
697 *ZmDeSI2*^{Hap1} transcription.

698 **Sequence and evolutionary analyses.** InterPro (https://www.ebi.ac.uk/interpro/) was
699 used to predict protein domains, while individual *ZmDeSI2* homologs were identified
700 by searching the NCBI website (**http://www.ncbi.nlm.nih.gov/**). The DNAMAN
701 software was used for sequence alignment, and maximum likelihood estimation
702 analyses were performed.

703 **Subcellular localization assays.** The localization of ZmDeSI2 within cells was

704 assessed by amplifying the full-length *ZmDeSI2* cDNA from B73 and inserting it into
705 the *35S:GFP* vector. After purifying the resultant constructs, they were used to
706 transform maize protoplasts. A Zeiss LSM700 laser scanning confocal microscope was
707 then used to detect the GFP fluorescent signal. The primers used for this analysis are
708 presented in Supplemental Table 9.

709 **qPCR.** A FastPure® Plant Total RNA Isolation Kit (Nanjing Vazyme Biotech Co. Ltd.,
710 China) was used to extract total RNA from 20 DAP endosperm samples, after which
711 FastKing gDNA Dispelling RT SuperMix (Tiangen Biotech Co. Ltd., China) was used
712 to prepare cDNA. A Bio-Rad iQ5 with Real-Time PCR System cycler (Applied
713 Biosystems) system was then used to perform qPCR analyses, with tubulin as a
714 normalization control. The primers used for this analysis are presented in Supplemental
715 Table 9.

716 **Luciferase complementation imaging (LCI) assay.** The *ZmDeSI2* CDS was cloned
717 into the transient pCAMBIA1300-nLUC expression vector, while all other candidate
718 proteins were cloned into the pCAMBIA1300-cLUC vector. These constructs were then
719 used to transform *Agrobacterium* strain GV3101 cells, followed by the co-infiltration
720 of different plasmid combinations into 4-week-old *N. benthamiana* leaves. After 48–96
721 hours, LUC activity in the infiltrated leaves was analyzed with a Tanon-5200 ECL
722 imager (Tanon, Shanghai, China). Primers used to prepare the plasmids in this assay are
723 listed in Supplemental Table 9.

724 **Pull-down assays.** The *ZmDeSI2*/*E2*/*ZmSUMO1a* and *ZmSIR* CDS were separately
725 cloned into the *Nde*I and *Xho*I sites in the pET-30a vector and the *Nde*I and *Xba*I sites

726 in the pCZN1 vector to generate the Flag-ZmDeSI2/E2/ZmSUMO1a and His-ZmSIR
727 fusion proteins. These constructs were used to transform *E. coli* BL21 (DE3), inducing
728 recombinant protein expression by adding 0.2 mM IPTG. Pull-down assays were
729 performed by combining Flag-tag purification resin (Beyotime) with Flag-
730 ZmDeSI2/E2/ZmSUMO1a and His-ZmSIR for 4 h at 4°C. The Ni Magarose Beads
731 were then washed using PBS (137 mM NaCl, 2.7 mM KCl, 10 mM Na_2HPO_4, 2 mM
732 KH_2PO_4, 0.05% SDS, 1% Triton X-100), separated via SDS-PAGE, and detected with
733 anti-DDDDK (FLAG) (1:5,000 dilution; Zoonbio Biotechnology Co. Ltd) or anti-His
734 (1:4,000; Zoonbio Biotechnology Co. Ltd), antibodies.

735 **BiFC assays.** The *ZmDeSI2*/*E2*/*ZmSUMO1a* CDS was cloned into the pXY104 vector
736 to produce the ZmDeSI2/E2/ZmSUMO1a-cYFP fusion protein. The *ZmSIR* CDS was
737 cloned into pXY106 to produce nYFP-ZmSIR. Each of these constructs was
738 transformed into *Agrobacterium* GV3101 cells and co-infiltrated into *N. benthamiana*
739 leaves based on appropriate experimental groupings. An LSM980 laser-scanning
740 confocal microscope (Carl Zeiss, Germany) was then used to detect fluorescent signals
741 in these leaves.

742 **IP-MS assay.** IP-MS was performed to identify potential downstream interacting
743 proteins. The total protein of *pUbi:ZmDeSI2-Flag* transgenic events was extracted
744 using a Plant Protein Extraction Kit (CWBIO, CW0885M) in the presence of protease
745 inhibitors at 4°C for 30 minutes. Lysates (5 mg protein) were incubated for 2 h at 25°C
746 with 200 μl of anti-DYDDDDK magnetic beads (Smart-Lifesciences, SM009001).
747 Antibody-protein complexes were captured using magnetic beads, washed three times

748 with PBS. The beads were denatured, separated by SDS-PAGE, and stained with
749 Coomassie Blue. The indicated bands were subsequently subjected to mass
750 spectrometry (MS) analysis (Applied Protein Technology, Shanghai, China). Specific
751 interactors were defined using the criterion of ⩾4-fold enrichment in test antibody
752 samples versus controls (adjusted $P<0.05$), with the exclusion of background proteins
753 common to both groups. The use of three biological replicates ensured reproducibility.
754 ***In vivo* SUMOylation conjugation analysis.** *Agrobacterium* GV3101 cells harboring
755 the *35S:ZmSIR-Flag* and *35S:ZmSUMO1a-Myc* constructs were used to infiltrate 4-
756 week-old *N. benthamiana* leaves. The ability of ZmDeSI2 to mediate ZmSIR
757 deSUMOylation was assessed by also including *35S:ZmDeSI2*-His in these analyses.
758 The transformed leaves were then homogenized, and the proteins therein were extracted
759 with a Plant Protein Extraction Kit (CWBIO, CW0885M) at 4°C for 30 minutes. These
760 proteins were then mixed with 10× SDS-PAGE loading buffer, separated on SDS-PAGE,
761 and transferred to membranes for immunoblotting with anti-DDDDK (FLAG) (1:2,000;
762 Abclone, China), anti-Myc (1:2,000; Abclone), and anti-His (1:2,000 dilution; Abclone).
763 ***In vitro* SUMOylation conjugation analysis.** Recombinant His-ZmSIR and Flag-
764 ZmDeSI2 were purified from *E. coli* BL21 (DE3). Next, 50 ng of purified E1 Myc-
765 ZmSAE1/2, 50 ng of purified E2 Myc-ZmSCE1, 1 μg of purified Myc-ZmSUMO1a,
766 0.5 μg of His-ZmSIR, and Flag-ZmDeSI2 were combined in 30 μL of reaction buffer
767 (2 mM ATP, 50 mM Tris–HCl, pH 7.5, and 5 mM $MgCl_2$) and incubated for 2 h at 30°C.
768 These proteins were then separated by SDS-PAGE and subjected to immunoblotting

769 analysis, with anti-His (1:1,000; Zoonbio Biotechnology Co. Ltd) being used to detect
770 SUMOylated His-ZmSIR.

771 ***In vivo* degradation assay**

772 The ZmSIR CDS was cloned into the pCAMBIA1300-Flag vector to produce the
773 pCAMBIA1300-ZmSIR-Flag construct. Then, 4-week-old *N. benthamiana* leaves were
774 co-transfected with combinations of empty vector (EV)-Myc + pCAMBIA1300-
775 ZmSIR-Flag, pCAMBIA1300-ZmSUMO1a-Myc + pCAMBIA1300-ZmSIR-Flag,
776 pCAMBIA1300-ZmSUMO1a-Myc + pCAMBIA1300-ZmSIR-Flag +
777 pCAMBIA1300-ZmDeSI2-His, pCAMBIA1300-ZmSIR-T-Flag + pCAMBIA1300-
778 Myc, and pCAMBIA1300-ZmSIR-T-Flag + pCAMBIA1300-ZmSUMO1a-Myc were
779 used for a ZmSIR protein degradation assay. ZmSIR-T represents the mutated sequence
780 of the SUMOylation site synthesized *in vitro*. ZmSIR-Flag/ ZmSIR-T-Flag-
781 containing extracts from the leaves in each group were incubated with ATP (1 mM) and
782 MG132 (100 μM). A Plant Protein Extraction Kit (CWBIO, CW0885M) was employed
783 to extract total protein from 0.1 g of plant tissue using 500 μL of extraction buffer,
784 following incubation at 4°C for 30 minutes after 48 or 96 hours. The proteins were
785 mixed with 10× SDS-PAGE loading buffer, separated on SDS-PAGE, and transferred
786 to membranes for immunoblotting with anti-Myc (1:2,000; Abclone). Actin was used
787 as a loading control.

788 **Cell-free protein degradation assay**

789 Cell-free protein degradation assays were performed with a slightly modified version
790 of a previously reported protocol (Kong et al., 2015). Briefly, degradation buffer was

791 used to extract total protein from WT and transgenic kernels, after which cell-free
792 protein degradation reactions were established by combining 500 μg of total protein
793 with 100 ng of ZmSIR-His purified from *E. coli* BL21 (DE3) cells. For experiments
794 focused on proteasome inhibition, the total protein samples were combined with 100
795 μM MG132 for 8 h prior to the cell-free degradation assay. Reactions were incubated
796 at 28°C, and mixed solutions were collected after 0, 2, 4, and 8 h for analysis via
797 immunoblotting with anti-His (1:2,000; Abclone). Results were quantified with ImageJ
798 1.46r (https://imagej.nih.gov/ij/index.html).

799 **Selection analysis.** Genetic differentiation fixation index (F_{ST}) (Wang et al., 2018b) and
800 the XP-CLR (Chen et al., 2010) scores were computed with VCFtools (0.1.13) using a
801 20 kb sliding window and a 2 kb sliding step to facilitate the identification of potential
802 selective signals for 264 inbred lines from the inbred line population (PA vs PB).
803 Candidate sweeps were identified as those chromosomal regions corresponding to the
804 top 5% of FST and XP-CLR scores.

805 **Statistics & reproducibility**

806 Data were presented as mean ± s.d. (standard deviation), and were analyzed with
807 GraphPad Prism 8.0. The numbers of biologically independent samples (n) for each
808 experiment are noted in the figure legends. Pairs *t*-tests conducted in SPSS were used
809 for statistical analyses.

810 **Data availability**

811 All materials in this study are available from the corresponding authors upon request.
812 The authors declare that all data supporting the findings of this study are available

813 within the article, supplementary information files, and source data. Primers used in
814 this study are provided in Supplemental Table 9. Sequence data generated in this study
815 have been deposited in the NCBI SRA database under accession number
816 PRJNA1175378 and the China National Genomics Data Center under accession
817 number CRA024776.

818 **Author contribution statement**

819 X. Lu performed the experiments and wrote the paper. Y.H. Lei, Z.N. Xu, Z.X. Cheng,
820 Y.X. Tai, X.H. Han, M. Liu, Z.F. Hao, M.S. Li, D.G. Zhang, H.J. Yong and J.N. Han,
821 Z.H. Wang, W.X. Li assisted with the experimental operations and advised the paper.
822 Z.Q. Zhou, J.F. Weng, and X.H. Li designed the experiments and revised the paper. All
823 authors contributed to the article and approved the submitted version.

824 **Acknowledgements**

825 This research was jointly funded by the National Natural Science Foundation of China
826 (32301797) and National Natural Science Foundation of China (32001559).
827 We also thank Novogene and Zoonbio Biotechnology Co. Ltd for technical support.

References

Alagawany, M., Abd El-Hack, M. E., Arif, M., and Ashour, E. A. (2016). Individual and combined effects of crude protein, methionine, and probiotic levels on laying hen productive performance and nitrogen pollution in the manure. *Environ. Sci. Pollut. Res. Int.*, **23**, 22906–22913. 10.1007/s11356-016-7511-6.

Alexander, D. H., Novembre, J., and Lange, K. (2009). Fast model-based estimation of ancestry in unrelated individuals. *Genome Res.*, **19**, 1655–1664. 10.1101/gr.094052.109.

Anjum, N. A., Gill, R., Kaushik, M., Hasanuzzaman, M., Pereira, E., Ahmad, I., Tuteja, N., and Gill, S. S. (2015). ATP-sulfurylase, sulfur-compounds, and plant stress tolerance. *Front. Plant Sci.*, **6**, 210. 10.3389/fpls.2015.00210.

Armbruster, L., Uslu, V. V., Wirtz, M., and Hell, R. (2019). The recovery from sulfur starvation is independent from the mRNA degradation initiation enzyme PARN in *Arabidopsis*. *Plants (Basel, Switzerland)*, **8**, 380. 10.3390/plants8100380.

Bates, D., Mchler, M., Bolker, B. M., and Walker, S. C. (2015). Fitting linear mixed-effects models using *lme4*. *Found. Open Access Stat.*, **67**, 1–48. 10.1007/0-387-22747-4_4.

Carvalho, T. S. M., Sousa, L. S., Nogueira, F. A., Vaz, D. P., Saldanha, M. M., Triginelli, M. V., Pinto, M., Baião, N. C., and Lara, L. J. C. (2018). Digestible methionine + cysteine in the diet of commercial layers and its influence on the performance, quality, and amino acid profile of eggs and economic evaluation. *Poult. Sci.*, **97**, 2044–2052. 10.3382/ps/pey036.

Chen, H., Patterson, N., and Reich, D. (2010). Population differentiation as a test for selective sweeps. *Genome Res.*, **20**, 393–402. 0.1101/gr.100545.109.

Chen, J., Zeng, B., Zhang, M., Xie, S., Wang, G., Hauck, A., and Lai, J. (2014). Dynamic transcriptome landscape of maize embryo and endosperm development. *Plant Physiol.*, **166**, 252–264. 10.1104/pp.114.240689.

Chia, J. M., Song, C., Bradbury, P. J., Costich, D., de Leon, N., Doebley, J., Elshire, R. J., Gaut, B., Geller, L., Glaubitz, J. C., et al. (2012). Maize HapMap2 identifies extant variation from a genome in flux. *Nat. Genet.*, **44**, 803–807. 10.1038/ng.2313.

Deng, M., Li, D., Luo, J., Xiao, Y., Liu, H., Pan, Q., Zhang, X., Jin, M., Zhao, M., and Yan, J. (2017). The genetic architecture of amino acids dissection by association and linkage analysis in maize. *Plant Biotechnol. J.*, **15**, 1250–1263. 10.1111/pbi.12712.

Devi, V., Bhushan, B., Gupta, M., Sethi, M., Kaur, C., Singh, A., Singh, V., Kumar, R., Rakshit, S., and Chaudhary, D. P. (2023). Genetic and molecular understanding for the development of methionine-rich maize: a holistic approach. *Front. Plant Sci.*, **14**, 1249230. 10.3389/fpls.2023.1249230.

Fuentes-Lara, L. O., Medrano-Macías, J., Pérez-Labrada, F., Rivas-Martínez, E. N., García-Enciso, E. L., González-Morales, S., Juárez-Maldonado, A., Rincón-Sánchez, F., and Benavides-Mendoza, A. (2019). From elemental sulfur to hydrogen sulfide in agricultural soils and plants. *Molecules (Basel, Switzerland)*, **24**, 2282. 10.3390/molecules24122282.

Goyal, P., Devi, R., Verma, B., Hussain, S., Arora, P., Tabassum, R., and Gupta, S. (2023). WRKY transcription factors: evolution, regulation, and functional diversity in plants. *Protoplasma*, **260**, 331–348. 10.1007/s00709-022-01794-7.

Guo, L., Wang, X., Zhao, M., Huang, C., Li, C., Li, D., Yang, C. J., York, A. M., Xue, W., Xu, G., et al. (2018). Stepwise cis-regulatory changes in ZCN8 contribute to maize flowering-time

adaptation. *Curr. Biol.*: **28**, 3005–3015.e3004. 10.1016/j.cub.2018.07.029.

Hawkesford, M. J. (2003). Transporter gene families in plants: The sulphate transporter gene family—redundancy or specialization? *Physiol. Plant.* **117**, 155–163. 10.1034/j.1399-3054.2003.00034.x.

Hay, R. T. (2005). SUMO: a history of modification. *Mol. Cell*, **18**, 1–12. 10.1016/j.molcel.2005.03.012.

Hay, R. T. (2013). Decoding the SUMO signal. *Biochem. Soc. Trans.*, **41**, 463–473. 10.1042/BST20130015.

Hendriks, I. A., and Vertegaal, A. C. (2016). A comprehensive compilation of SUMO proteomics. *Nat. Rev. Mol. Cell Biol.*, **17**, 581–595. 10.1038/nrm.2016.81.

Herrmann, J., Ravilious, G. E., McKinney, S. E., Westfall, C. S., Lee, S. G., Baraniecka, P., Giovannetti, M., Kopriva, S., Krishnan, H. B., and Jez, J. M. (2014). Structure and mechanism of soybean ATP sulfurylase and the committed step in plant sulfur assimilation. *J. Biol. Chem.*, **289**, 10919–10929. 10.1074/jbc.M113.540401.

Huang, Y., Wang, H., Zhu, Y., Huang, X., Li, S., Wu, X., Zhao, Y., Bao, Z., Qin, L., Jin, Y., et al. (2022). THP9 enhances seed protein content and nitrogen-use efficiency in maize. *Nature*, **612**, 292–300. 10.1038/s41586-022-05441-2.

Jackson, T. L., Baker, G. W., Wilks, F. R., Jr., Popov, V. A., Mathur, J., and Benfey, P. N. (2015). Large cellular inclusions accumulate in *Arabidopsis* roots exposed to low-sulfur conditions. *Plant Physiol.*, **168**, 1573–1589. 10.1104/pp.15.00465.

Jez, J. M. (2019). Structural biology of plant sulfur metabolism: from sulfate to glutathione. *J. Exp. Bot.*, **70**, 4089–4103. 10.1093/jxb/erz094.

Jiang, J., Ma, S., Ye, N., Jiang, M., Cao, J., and Zhang, J. (2017). WRKY transcription factors in plant responses to stresses. *J. Integr. Plant Biol.*, **59**, 86–101. 10.1111/jipb.12513.

Jiang, L., Wang, Y., Xia, A., Wang, Q., Zhang, X., Jez, J. M., Li, Z., Tan, W., and He, Y. (2021). A natural single-nucleotide polymorphism variant in sulfite reductase influences sulfur assimilation in maize. *New Phytol.*, **232**, 692–704. 10.1111/nph.17616.

Jiao, Y., Peluso, P., Shi, J., Liang, T., Stitzer, M. C., Wang, B., Campbell, M. S., Stein, J. C., Wei, X., Chin, C. S., et al. (2017). Improved maize reference genome with single-molecule technologies. *Nature*, **546**, 524–527. 10.1038/nature22971.

Jiao, Y., Zhao, H., Ren, L., Song, W., Zeng, B., Guo, J., Wang, B., Liu, Z., Chen, J., Li, W., et al. (2012). Genome-wide genetic changes during modern breeding of maize. *Nat. Genet.*, **44**, 812–815. 10.1038/ng.2312.

Joo, H., Baek, W., Lim, C. W., and Lee, S. C. (2024). Pepper SUMO protease CaDeSI2 positively modulates the drought responses via deSUMOylation of clade A PP2C CaAITP1. *New Phytol.*, **243**, 1361–1373. 10.1111/nph.19920.

Kang, H. M., Sul, J. H., Service, S. K., Zaitlen, N. A., Kong, S. Y., Freimer, N. B., Sabatti, C., and Eskin, E. (2010). Variance component model to account for sample structure in genome-wide association studies. *Nat. Genet.*, **42**, 348–354. 10.1038/ng.548.

Khan, M. S., Haas, F. H., Samami, A. A., Gholami, A. M., Bauer, A., Fellenberg, K., Reichelt, M., Hänsch, R., Mendel, R. R., Meyer, A. J., et al. (2010). Sulfite reductase defines a newly discovered bottleneck for assimilatory sulfate reduction and is essential for growth and development in *Arabidopsis thaliana*. *Plant Cell*, **22**, 1216–1231. 10.1105/tpc.110.074088.

Kong, L., Cheng, J., Zhu, Y., Ding, Y., Meng, J., Chen, Z., Xie, Q., Guo, Y., Li, J., Yang, S., et

al. (2015). Degradation of the ABA co-receptor ABI1 by PUB12/13 U-box E3 ligases. *Nat. Commun.*, **6**, 8630. 10.1038/ncomms9630.

Kopriva, S., Malagoli, M., and Takahashi, H. (2019). Sulfur nutrition: impacts on plant development, metabolism, and stress responses. *J. Exp. Bot.*, **70**, 4069–4073. 10.1093/jxb/erz319.

Koprivova, A., and Kopriva, S. (2016). Sulfur metabolism and its manipulation in crops. *J. Genet. Genomics*, **43**, 623–629. 10.1016/j.jgg.2016.07.001.

Leustek, T. (2002). Sulfate metabolism. *The Arabidopsis Book*, **1**, e0017. 10.1199/tab.0017.

Li, C., Guan, H., Jing, X., Li, Y., Wang, B., Li, Y., Liu, X., Zhang, D., Liu, C., Xie, X., et al. (2022). Genomic insights into historical improvement of heterotic groups during modern hybrid maize breeding. *Nat. Plants*, **8**, 750–763. 10.1038/s41477-022-01190-2.

Li, C., Li, Y., Song, G., Yang, D., Xia, Z., Sun, C., Zhao, Y., Hou, M., Zhang, M., Qi, Z., et al. (2023a). Gene expression and expression quantitative trait loci analyses uncover natural variations underlying the improvement of important agronomic traits during modern maize breeding. *Plant J.*, **115**, 772–787. 10.1111/tpj.16260.

Li, C., Yue, Y., Chen, H., Qi, W., and Song, R. (2018a). The ZmbZIP22 transcription factor regulates 27-kD γ-zein gene transcription during maize endosperm development. *Plant Cell*, **30**, 2402–2424. 10.1111/tpj.16260.

Li, H., and Durbin, R. (2009). Fast and accurate short read alignment with Burrows-Wheeler transform. *Bioinformatics*, **25**, 1754–1760. 10.1093/bioinformatics/btp324.

Li, H., Peng, Z., Yang, X., Wang, W., Fu, J., Wang, J., Han, Y., Chai, Y., Guo, T., Yang, N., et al. (2013). Genome-wide association study dissects the genetic architecture of oil biosynthesis in maize kernels. *Nat. Genet.*, **45**, 43–50. 10.1038/ng.2484.

Li, L., Tian, Z., Chen, J., Tan, Z., Zhang, Y., Zhao, H., Wu, X., Yao, X., Wen, W., Chen, W., et al. (2023b). Characterization of novel loci controlling seed oil content in *Brassica napus* by marker metabolite-based multi-omics analysis. *Genome Biol.*, **24**, 141. 10.1186/s13059-023-02984-z.

Li, S. J., and Hochstrasser, M. (1999). A new protease required for cell-cycle progression in yeast. *Nature*, **398**, 246–251. 10.1038/18457.

Li, X., Han, Y., Yan, Y., Messing, J., and Xu, J. H. (2018b). Genetic diversity and evolution of reduced sulfur storage during domestication of maize. *Plant J.*, **94**, 943–955. 10.1111/tpj.13907.

Lin, R., Ding, L., Casola, C., Ripoll, D. R., Feschotte, C., and Wang, H. (2007). Transposase-derived transcription factors regulate light signaling in *Arabidopsis*. *Science*, **318**, 1302–1305. 10.1126/science.

Liu, H., Wang, F., Xiao, Y., Tian, Z., Wen, W., Zhang, X., Chen, X., Liu, N., Li, W., Liu, L., et al. (2016). MODEM: multi-omics data envelopment and mining in maize. *Database*, **2016**, baw117. 10.1093/database/baw117.

Ma, Y., Min, L., Wang, J., Li, Y., Wu, Y., Hu, Q., Ding, Y., Wang, M., Liang, Y., Gong, Z., et al. (2021). A combination of genome-wide and transcriptome-wide association studies reveals genetic elements leading to male sterility during high temperature stress in cotton. *New Phytol.*, **231**, 165–181. 10.1111/nph.17325.

Mabb, A. M., Wuerzberger-Davis, S. M., and Miyamoto, S. (2006). PIASy mediates NEMO sumoylation and NF-κB activation in response to genotoxic stress. *Nat. Cell Biol.*, **8**, 986–993.

10.1111/nph.17325.

Mao, H., Wang, H., Liu, S., Li, Z., Yang, X., Yan, J., Li, J., Tran, L. S., and Qin, F. (2015). A transposable element in a NAC gene is associated with drought tolerance in maize seedlings. *Nat. Commun.*, **6**, 8326. 10.1038/ncomms9326.

Maruyama-Nakashita, A. (2017). Metabolic changes sustain the plant life in low-sulfur environments. *Curr. Opin. Plant Biol.*, **39**, 144–151. 10.1016/j.pbi.2017.06.015.

Mertz, E. T., Bates, L. S., and Nelson, O. E. (1964). Mutant gene that changes protein composition and increases lysine content of maize endosperm. *Science*, **145**, 279–280. 10.1016/j.pbi.2017.06.015.

Morrell, R., and Sadanandom, A. (2019). Dealing with stress: A review of plant SUMO proteases. *Front. Plant Sci.*, **10**, 1122. 10.3389/fpls.2019.01122.

Nelson, O. E., Mertz, E. T., and Bates, L. S. (1965). Second mutant gene affecting the amino acid pattern of maize endosperm proteins. *Science*, **150**, 1469–1470. 10.1126/science.150.3702.1469.

Novatchkova, M., Budhiraja, R., Coupland, G., Eisenhaber, F., and Bachmair, A. (2004). SUMO conjugation in plants. *Planta*, **220**, 1–8. 10.1007/s00425-004-1370-y.

Okada, S., Nagabuchi, M., Takamura, Y., Nakagawa, T., Shinmyozu, K., Nakayama, J., and Tanaka, K. (2009). Reconstitution of *Arabidopsis thaliana* SUMO pathways in *E. coli*: functional evaluation of SUMO machinery proteins and mapping of SUMOylation sites by mass spectrometry. *Plant Cell Physiol.*, **50**, 1049–1061. 10.1093/pcp/pcp056.

Olsen, M., Krone, T., and Phillips, R. (2003). BSSS53 as a donor source for increased whole-kernel methionine in maize. *Crop Sci.*, **43**, 1634–1642. 10.2135/cropsci2003.1634.

Orosa, B., Yates, G., Verma, V., Srivastava, A. K., Srivastava, M., Campanaro, A., De Vega, D., Fernandes, A., Zhang, C., Lee, J., et al. (2018). SUMO conjugation to the pattern recognition receptor FLS2 triggers intracellular signalling in plant innate immunity. *Nat. Commun.*, **9**, 5185. 10.1038/s41467-018-07696-8.

Panthee, D. R., Pantalone, V. R., Sams, C. E., Saxton, A. M., West, D. R., Orf, J. H., and Killam, A. S. (2006). Quantitative trait loci controlling sulfur-containing amino acids, methionine and cysteine, in soybean seeds. *Theor. Appl. Genet.*, **112**, 546–553. 10.1007/s00122-005-0161-6.

Planta, J., Xiang, X., Leustek, T., and Messing, J. (2017). Engineering sulfur storage in maize seed proteins without apparent yield loss. *Proc. Natl. Acad. Sci. U.S.A.*, **114**, 11386–11391. 10.1073/pnas.1714805114.

Price, A. L., Patterson, N. J., Plenge, R. M., Weinblatt, M. E., Shadick, N. A., and Reich, D. (2006). Principal components analysis corrects for stratification in genome-wide association studies. *Nat. Genet.*, **38**, 904–909. 10.1038/ng1847.

Purcell, S., Neale, B., Todd-Brown, K., Thomas, L., Ferreira, M. A., Bender, D., Maller, J., Sklar, P., de Bakker, P. I., Daly, M. J., et al. (2007). PLINK: a tool set for whole-genome association and population-based linkage analyses. *Am. J. Hum. Genet.*, **81**, 559–575. 10.1086/519795.

Rushton, D. L., Tripathi, P., Rabara, R. C., Lin, J., Ringler, P., Boken, A. K., Langum, T. J., Smidt, L., Boomsma, D. D., Emme, N. J., et al. (2012). WRKY transcription factors: key components in abscisic acid signalling. *Plant Biotechnol. J.*, **10**, 2–11. 10.1111/j.1467-7652.2011.00634.x.

Sang, Q., and Kong, F. J. N. C. (2024). Applications for single-cell and spatial transcriptomics in

plant research. *New Crops*, **1**, 100025. 10.1016/j.ncrops.2024.100025

Shi B, Li K, Xu R, Zhang F, Yu Z, Ding Z, Tian H. (2025). Methionine-mediated trade-off between plant growth and salt tolerance. *Plant Physiol*. **197**, kiaf074. 10.1093/plphys/kiaf074.

Shin, E. J., Shin, H. M., Nam, E., Kim, W. S., Kim, J. H., Oh, B. H., and Yun, Y. (2012). DeSUMOylating isopeptidase: a second class of SUMO protease. *EMBO Rep.*, **13**, 339–346. 10.1038/embor.2012.3.

Su, W., Gu, X., and Peterson, T. (2019). TIR-Learner, a new ensemble method for TIR transposable element annotation, provides evidence for abundant new transposable elements in the maize genome. *Mol. Plant*, **12**, 447–460. 10.1016/j.molp.2019.02.008.

Sun, S. C. (2008). Deubiquitylation and regulation of the immune response. *Nat. Rev. Immunol.*, **8**, 501–511. 10.1038/nri2337.

Sveier, Nordås, Berge, and Lied. (2001). Dietary inclusion of crystalline D- and L-methionine: effects on growth, feed and protein utilization, and digestibility in small and large Atlantic salmon (*Salmo salar* L.). *Aquacult. Nutr.*, **7**, 501–511. 10.1038/nri2337.

Tang, S., Zhao, H., Lu, S., Yu, L., Zhang, G., Zhang, Y., Yang, Q. Y., Zhou, Y., Wang, X., Ma, W., et al. (2021). Genome- and transcriptome-wide association studies provide insights into the genetic basis of natural variation of seed oil content in *Brassica napus*. *Mol. Plant*, **14**, 470–487. 10.1016/j.molp.2020.12.003.

Tian, J., Wang, C., Xia, J., Wu, L., Xu, G., Wu, W., Li, D., Qin, W., Han, X., Chen, Q., et al. (2019). Teosinte ligule allele narrows plant architecture and enhances high-density maize yields. *Science*, **365**, 658–664. 10.1126/science.aax5482.

Vierstra, R. D. (2012). The expanding universe of ubiquitin and ubiquitin-like modifiers. *Plant Physiol.*, **160**, 2–14. 10.1104/pp.112.200667.

Wang, B., Lin, Z., Li, X., Zhao, Y., Zhao, B., Wu, G., Ma, X., Wang, H., Xie, Y., Li, Q., et al. (2020). Genome-wide selection and genetic improvement during modern maize breeding. *Nat. Genet.*, **52**, 565–571. 10.1038/s41588-020-0616-3.

Wang, C. T., Ru, J. N., Liu, Y. W., Li, M., Zhao, D., Yang, J. F., Fu, J. D., and Xu, Z. S. (2018a). Maize WRKY transcription factor ZmWRKY106 confers drought and heat tolerance in transgenic plants. *Int. J. Mol. Sci.*, **19**, 3046. 10.3390/ijms19103046.

Wang, K., Li, M., and Hakonarson, H. (2010). ANNOVAR: functional annotation of genetic variants from high-throughput sequencing data. *Nucleic Acids Res.*, **38**, e164. 10.1093/nar/gkq603.

Wang, M., Li, W., Fang, C., Xu, F., Liu, Y., Wang, Z., Yang, R., Zhang, M., Liu, S., Lu, S., et al. (2018b). Parallel selection on a dormancy gene during domestication of crops from multiple families. *Nat. Genet.*, **50**, 1435–1441. 10.1038/s41588-018-0229-2.

Wang, X., Jiang, G. L., Song, Q., Cregan, P. B., Scott, R. A., Zhang, J., Yen, Y., and Brown, M. (2015). Quantitative trait locus analysis of seed sulfur-containing amino acids in two recombinant inbred line populations of soybean. *Euphytica*, **201**, 293–305. 10.1007/s10681-014-1223-0.

Wang, X., Wang, H., Liu, S., Ferjani, A., Li, J., Yan, J., Yang, X., and Qin, F. (2016). Genetic variation in ZmVPP1 contributes to drought tolerance in maize seedlings. *Nat. Genet.*, **48**, 1233–1241. 10.1038/ng.3636.

Wang, Y., and Wen, J. (2024). Available strategies for improving the biosynthesis of methionine: A review. *J. Agric. Food Chem.*, **72**, 17166–17175. 10.1021/acs.jafc.4c02728.

Xia, Z., Wang, M., and Xu, Z. (2018). The maize sulfite reductase is involved in cold and oxidative stress responses. *Front. Plant Sci.*, **9**, 1680. 10.3389/fpls.2018.01680.

Xiang, X., Wu, Y., Planta, J., Messing, J., and Leustek, T. (2018). Overexpression of serine acetyltransferase in maize leaves increases seed-specific methionine-rich zeins. *Plant Biotechnol. J.*, **16**, 1057–1067. 10.1111/pbi.12851.

Yan, P., Du, Q., Chen, H., Guo, Z., Wang, Z., Tang, J., and Li, W. X. (2023). Biofortification of iron content by regulating a NAC transcription factor in maize. *Science*, **382**, 1159–1165. 10.1126/science.adf3256.

Yang, J., Fu, M., Ji, C., Huang, Y., and Wu, Y. (2018). Maize oxalyl-CoA decarboxylase1 degrades oxalate and affects the seed metabolome and nutritional quality. *Plant Cell*, **30**, 2447–2462. 10.1126/science.adf3256.

Yang, Q., Li, Z., Li, W., Ku, L., Wang, C., Ye, J., Li, K., Yang, N., Li, Y., Zhong, T., et al. (2013). CACTA-like transposable element in *ZmCCT* attenuated photoperiod sensitivity and accelerated the postdomestication spread of maize. *Proc. Natl. Acad. Sci. U.S.A.*, **110**, 16969–16974. 10.1073/pnas.1310949110.

Yang Z, Cao Y, Shi Y, Qin F, Jiang C, Yang S. (2023). Genetic and molecular exploration of maize environmental stress resilience: Toward sustainable agriculture. *Mol Plant.* **16**,1496-1517. 10.1016/j.molp.2023.07.005.

Yarmolinsky, D., Brychkova, G., Kurmanbayeva, A., Bekturova, A., Ventura, Y., Khozin-Goldberg, I., Eppel, A., Fluhr, R., and Sagi, M. (2014). Impairment in sulfite reductase leads to early leaf senescence in tomato plants. *Plant Physiol.*, **165**, 1505–1520. 10.1073/pnas.1310949110.

Zhang, J., Zuo, T., Wang, D., and Peterson, T. (2014). Transposition-mediated DNA re-replication in maize. *eLife*, **3**, e03724. 10.7554/eLife.03724.

Zhang, M., Cao, Y., Wang, Z., Wang, Z. Q., Shi, J., Liang, X., Song, W., Chen, Q., Lai, J., and Jiang, C. (2018). A retrotransposon in an HKT1 family sodium transporter causes variation of leaf Na^+ exclusion and salt tolerance in maize. *New Phytol.*, **217**, 1161–1176. 10.1111/nph.14882.

Zhang, Y., Zhang, H., Zhao, H., Xia, Y., Zheng, X., Fan, R., Tan, Z., Duan, C., Fu, Y., Li, L., et al. (2022). Multi-omics analysis dissects the genetic architecture of seed coat content in *Brassica napus*. *Genome Biol.*, **23**, 86. 10.1186/s13059-022-02647-5.

Zhou, Y., Cai, H., Xiao, J., Li, X., Zhang, Q., and Lian, X. (2009). Over-expression of aspartate aminotransferase genes in rice resulted in altered nitrogen metabolism and increased amino acid content in seeds. *Theor. Appl. Genet.*, **118**, 1381–1390. 10.1007/s00122-009-0988-3.

Figure legends

Figure 1. GWAS analysis of kernel Met content in inbred maize lines.
(A) Phenotypic variations in the kernel Met levels in the analyzed population of inbred maize lines. Histograms within the block show the distribution of phenotypic BLUE values corresponding to Met content. The red and green curves respectively represent the actual phenotypic distribution and the normal distribution.
(B) The population structure of the inbred maize population used for this study. The inbred lines were classified into five groups, including PB, LAN, SPT, BSSS, and PA respectively represented by PH4CV, Mo17, HuangZaoSi, B73, and Zheng58.
(C) PCA plots of the first and third principal components (PCs). Different colors and shapes are used to represent inbred lines from different eras.
(D) GWAS analysis of maize kernel Met content BLUE values based on data from the 264-inbred maize lines population [(-log10(*P*)=5.0].
(E) Analysis of correlations between *ZmDeSI2* expression and kernel Met levels in the populations of inbred maize lines.
(F) Local Manhattan plot (upper) and LD heatmap (lower) around the peak on chromosome 2. The candidate region for the peak is represented with red dashed lines, while the linkage between *ZmDeSI2* nucleotide variations and peak are shown in the triangle plot.
(G-H) Kernel Met content **(G)** and *ZmDeSI2* expression **(H)** in $ZmDeSI2^{Hap1}$ and $ZmDeSI2^{Hap2}$. Statistical significance indicated by *P*-values was determined by paired *t*-tests. Error bars indicate mean ± s.d.

Figure 2. *ZmDeSI2* functions as a negative regulator of maize kernel Met content.
(A) *ZmDeSI2* variant sites generated through CRISPR-Cas9 editing and in EMS mutants.
(B-C) PCR-based sequencing was used to verify mutated nucleotides. The mutation site is represented in blue, and the premature stop codon is indicated. The dashed lines and numbers represent the positions of the detected primer mutation sites.
(D) Kernel Met levels in EMS-derived *desi2* mutants of the BC_2F_2 and BC_3F_2 generations. Statistical significance indicated by *P*-values was determined by paired *t*-tests. Error bars indicate mean ± s.d.
(E) Schematic diagram of the *pUbi:ZmDeSI2-Flag* overexpression construct.
(F) Reduced Met levels in the kernels of *ZmDeSI2*-overexpression lines. Statistical significance indicated by *P*-values was determined by paired *t*-tests. Error bars indicate mean ± s.d.
(G) Target sites of *ZmDeSI2* mutants generated through CRISPR-Cas9 editing and indicated by dashed lines. -2/-3 bp for CR#1 indicates a 2-bp deletion at the first target site and a 3-bp deletion at the second target site.
(H) Images (scale bars = 1 cm) of *ZmDeSI2* mutants generated through CRISPR-Cas9 editing.
(I) Kernel Met content in the B73, CR1, and CR2 lines. Statistical significance indicated by *P*-values was determined by paired *t*-tests. Error bars indicate mean ± s.d.
(J-O) Statistics for hundred kernel weight (HKW) **(J)**, number of rows per ear (RN) **(K)**, number of kernels per row (KNPR) **(L)**, kernel length (KL) **(M)**, kernel width (KW) **(N)**, kernel thickness (KT) **(O)** of wild-type (B73) and CRISPR-knockout (CR#1 and CR#2) plants. Dots indicate individual plants (nB73 = 3, nCR#1 = 3, nCR#2 = 3 in I; and nB73 = 10, nCR#1 = 10, nCR#2 = 10 in J-O). Statistical significance indicated by *P*-values was determined by paired *t*-tests. Error bars indicate mean ± s.d.

Figure 3. ZmWRKY105 positively regulates *ZmDeSI2* expression.

(A) Comparison of *ZmDeSI2*^{Hap1} promoter activity from the transcription start site of 250, 500, 750, 1000, and 1500 bp sections in *N. benthamiana* leaves. Higher levels of luciferase activity are denoted by a larger proportion of white area.

(B) Manhattan plots corresponding to the eQTL results for *ZmDeSI2* expression (TPM) in 348 inbred lines. The 10 maize chromosomes are represented using different colors. The genomic location of the *ZmDeSI2* and ZmWRKY105 association signal is marked with an arrow. The threshold [(-log10(*P*)=7.08] is marked with a gray dotted line.

(C) Y1H analyses demonstrating the binding of ZmWRKY105 to the *ZmDeSI2* promoter. Owing to the self-activation of the *ZmDeSI2*^{Hap1} promoter sequence, the truncated sequence was analyzed. S1 to S15 represent 1500 bp from the transcriptional start site in the *ZmDeSI2* ^{Hap1} promoter, with each fragment being 100 bp in size. *ZmDeSI2*^{Hap2}-Pro represents the promoter sequence of *ZmDeSI2*^{Hap2} with a length of 374 bp. The predicted taGTCAAa binding motif was located on S9.

(D) EMSA analyses demonstrating the binding of ZmWRKY105 to the *ZmDeSI2*^{Hap1} promoter tgGTCAAa motif and the effects of unlabeled probe-based competition. Lanes 1 and 2 represent positive controls, confirming proper probe labeling and binding under the experimental conditions. Lane 3 represents the *ZmDeSI2* promoter region probe, while Lane 4 illustrates the binding of ZmWRKY105 to this probe. Lanes 5 and 6 include cold probe competition assays, where unlabeled probes competed with labeled probes to verify the binding specificity. Lane 7 shows a mutated *ZmDeSI2* promoter region where the WRKY105 binding motif (GGTCAA) was disrupted, abolishing ZmWRKY105 binding. Lane 8 represents a negative control, containing ZmWRKY105 protein in the absence of probe, confirming the absence of non-specific signals.

(E) EMSA analyses demonstrating the binding of ZmWRKY105 to the *ZmDeSI2*^{Hap1} promoter S1, S3, S5, S7, S10, S11, S12, S13 and S15 fragments. Lane 10 acted as a negative control, only containing ZmWRKY105 protein, confirming no nonspecific signal.

(F) CUT&Tag-qPCR results demonstrating the direct binding of ZmWRKY105 to the 1-100 bp (S1), 800-900 bp (S9), and 1400-1500 bp (S15) segments from the transcriptional start site of the *ZmDeSI2*^{Hap1} promoter, with the value of each independent replicate represented by a dot. Since the average fragment size after digestion by transposase was between 250 and 500 bp, only distal sequences from S9 showing self-activation were selected for CUT&Tag-qPCR to minimize false positives. *ZmDeSI2*-Exon4 represents a designed primer targeting Exon 4 of *ZmDeSI2* and was used as a negative control. *ZmDeSI2*^{Hap2}-Pro represents the promoter sequence of ZmDeSI2^{Hap2} with a length of 374 bp. Mock indicates the negative control without GFP antibody. Statistical significance indicated by *P*-values was determined by paired *t*-tests. Error bars indicate mean ± s.d.

(G) Comparison of the effects of ZmWRKY105 and an empty vector on *ZmDeSI2*^{Hap1} and *ZmDeSI2*^{Hap2} promoter activity in *N. benthamiana* leaves. Higher levels of luciferase activity are denoted by a larger proportion of white area.

1177 **(H-I)** Protoplast dual-LUC reporter assays demonstrating the ability of ZmWRKY105
1178 to promote *ZmDeSI2*^{Hap1} promoter activation. Control cells were co-transfected with
1179 the reporter construct and an empty effector construct (n = 3 replicates). Statistical
1180 significance indicated by *P*-values was determined by paired *t*-tests. Error bars indicate
1181 mean ± s.d.
1182 **(J)** *ZmDeSI2* expression levels in endosperm samples from B73 and *wrky105* mutants
1183 collected 20 days after pollination (*P*=0.000433). Statistical significance indicated by
1184 *P*-values was determined by paired *t*-tests. Error bars indicate mean ± s.d.
1185 **(K)** Kernel Met content in the B73 and *wrky105* lines (*P*=3.3e-07). Statistical
1186 significance indicated by *P*-values was determined by paired *t*-tests. Error bars
1187 represent mean ± s.d.
1188

1189 **Figure 4. ZmDeSI2 functional analysis and substrate screening.**
1190 **(A)** Domain location analysis of the *ZmDeSI2* CDS region and a schematic overview
1191 of the mechanistic function of this deSUMOylating isopeptidase protein.
1192 **(B)** Sequence alignment of ZmDeSI2 and the orthologous human sequence,
1193 highlighting the conservation of the deSUMOylating isopeptidase domains.
1194 **(C)** Subcellular localization analyses of ZmDeSI2 in maize protoplasts. The control
1195 (*35S:GFP*) and *35S:ZmDeSI2-GFP* vectors were introduced into protoplasts.
1196 Brightfield, GFP, and merged images are shown from left to right. Scale bars = 5 μm.
1197 **(D)** The target gene of ZmDeSI2 action (Met metabolic pathway enzyme) was
1198 identified using LCI assays.
1199 **(E-G)** BiFC **(E, F)** and pull-down assays **(G)** demonstrating interactions between
1200 ZmDeSI2 and ZmSIR.
1201 **(H)** LCI assay revealed the interaction of ZmSIR with E2 in *N. benthamiana* leaves.
1202 **(I)** BiFC assays using a split YFP system in *N. benthamiana* leaves revealed the ability
1203 of ZmSIR-YFP^n and E2-YFP^c to interact.
1204 **(J)** Pull-down assays demonstrating the *in vitro* interactions between ZmSIR and E2.
1205 Protein mixtures were immunoprecipitated using the ProteinIso His Resin and detected
1206 using anti-Flag (upper) and anti-His (lower).
1207

1208

1209 **Figure 5. ZmDeSI2 mediates the deSUMOylation of ZmSIR.**

1210 **(A)** ZmDeSI2 mediates deSUMOylation of ZmSIR *in vitro.* Purified ZmSIR-His fusion
1211 protein (10 mM) from *E. coli* BL21 (DE3) were subjected to *in vitro* SUMOylation in
1212 the presence of E1, E2, and ZmSUMO1a, after which SUMOylated ZmSIR was
1213 incubated with 0, 4, 8, or 12 μg of ZmDeSI2 prepared from *E. coli* BL21 (DE3) at 37°C
1214 for 1 h. The reaction mixture was then immunoblotted with an anti-His antibody. The
1215 position of SUMOylated ZmDeSI2 is indicated by an arrow. Lane1 and 2 indicates that
1216 neither ZmSIR nor ZmSUMO1a undergoes SUMOylation when present separately.
1217 Lane 3 demonstrates that when E1, E2 and ZmSUMO1a are present together, ZmSIR
1218 can undergo SUMO modification. Lanes 4-6 show that ZmDeSI2 reduces both the
1219 SUMO modification and the protein stability of ZmSIR. As the concentration of
1220 ZmDeSI2 increases, the degree of SUMOylation of ZmSIR decreases, resulting in
1221 reduced protein stability.

1222 **(B)** ZmDeSI2 mediates the deSUMOylation of ZmSIR *in vivo. N. benthamiana* leaves
1223 co-expressing *ZmSIR-Flag* with *35S:Myc*; *35S:ZmSIR-Flag* with *35S:ZmSUMO1a-*
1224 *Myc*; *35S:ZmSIR-Flag* and *35S:ZmSUMO1a-Myc* with *35S:ZmDeSI2-His*; *ZmSIR*-T-
1225 *Flag* with *35S:Myc*; and *35S:ZmSIR*-T-*Flag* with *35S:ZmSUMO1a-Myc* were
1226 processed to extract proteins, which were subsequently immunoprecipitated with anti-
1227 Flag beads, after which anti-Myc, anti-Flag, anti-His, and anti-Actin antibodies were
1228 used for immunoblotting.

1229 **(C)** ZmSIR protein levels of B73, *desi2* mutants, and OE-*ZmDeSI2* transgenic lines.
1230 Total proteins extracted from the seeds of B73, *desi2* mutants, and OE-*ZmDeSI2*
1231 transgenic lines were precipitated with anti-ZmSIR or anti-Actin antibodies in western
1232 blotting analyses. Actin represented the loading control. ZmSIR protein levels were
1233 visualized by western blotting using an anti-ZmSIR antibody (ABclonal).

1234 **(D-E)** Crude extracts from *N. benthamiana* leaves co-expressing *ZmSIR-Flag* with
1235 *35S:Myc*; *35S:ZmSIR-Flag* with *35S:ZmSUMO1a-Myc*; *35S:ZmSIR-Flag* and
1236 *35S:ZmSUMO1a-Myc* with *35S:ZmDeSI2-His*; *ZmSIR*-T-*Flag* with *35S:Myc*; and
1237 *35S:ZmSIR*-T-*Flag* with *35S:ZmSUMO1a-Myc* were used for a ZmSIR protein
1238 degradation assay. ZmSIR-T represents the mutated sequence of the SUMOylation site
1239 synthesized *in vitro.* ZmSIR-Flag/ ZmSIR-T-Flag-containing extracts from the leaves
1240 in each group were incubated with ATP **(D)** and MG132 **(E)** for 2, 4, 6, or 8 h, after
1241 which anti-Flag (upper) and anti-Actin (middle) were used for immunoblotting, with
1242 Coomassie Brilliant Blue (CBB) staining (lower) confirming equal crude extract
1243 loading. Initial protein amounts prior to digestion are shown in the middle and lower
1244 panels.

1245 **(F-G)** ZmSIR protein degradation rates were measured after treatment using ATP **(F)**
1246 and MG132 **(G)**. Relative ZmSIR-Flag protein intensity levels were quantified with
1247 ImageJ 1.46r, with the protein levels at 0 h having been set to a value of 1.00 to enable
1248 the quantification of relative band intensity.

1249 **(H-I)** Cell-free ZmSIR-His degradation assays were performed with protein extracts
1250 from the WT (B73) and *desi2*-1 and *desi2*-2 mutants after incubation for 0, 2, 4, or 8 h
1251 with ATP **(H)** or 100 μM MG132 **(I)**. Anti-His was used for the immunoblotting-based

1252 detection of ZmSIR-His, with Actin as a loading control. The 0-h protein band was set
1253 to 1.00 to enable the quantification of relative band intensity.
1254 **(J-K)** ZmSIR-His degradation rates when incubated with protein extracts from WT
1255 (B73) and *desi2*-1 and *desi2*-2 mutants following treatment with ATP **(J)** and MG132
1256 **(K)**.
1257 **(L-M)** Cell-free ZmSIR-His degradation assays were performed with protein extracts
1258 from the WT (B73) and *OE-ZmDeSI2* lines mutants after incubation for 0, 2, 4, or 8 h
1259 with ATP **(L)** or 100 μM MG132 **(M)**. An anti-His antibody was used for the
1260 immunoblotting-based detection of ZmSIR-His, with Actin used as a loading control.
1261 The 0-h protein band was set to 1.00 to enable the quantification of relative band
1262 intensity.
1263 **(N-O)** ZmSIR-His degradation rates when incubated with protein extracts from WT
1264 (B73) and *OE-ZmDeSI2* lines following treatment with ATP **(N)** and MG132 **(O)**.
1265 ZmSIR degradation rates in **(F, G, J, K, N, and O)** are presented as mean ± s.d. (n=3).
1266

Figure 6. Marker–assisted selection of maize varieties with Met-enriched kernels.
(A) Phenotypic distributions of Met content in inbred lines across different heterotic groups. Significant differences are indicated by different letters above boxes for pairwise comparisons ($P < 0.05$, Bonferroni correction).
(B) *ZmDeSI2* haplotype distributions in five groups of inbred lines. The *ZmDeSI2*^{Hap1} and *ZmDeSI2*^{Hap2} percentage ratios are represented with pie charts.
(C-D) XP-CLR **(C)** and F_{ST} **(D)** for *ZmDeSI2* in the PA and PB groups. The location of *ZmDeSI2* is marked with red rectangles.
(E) *ZmDeSI2* allelic variation and molecular marker development.
(F-G) Met content **(F)** and gene expression levels **(G)** for haplotypes identified with the developed *ZmDeSI2* markers in 40 inbred lines not classified using resequencing data. Statistical significance indicated by *P*-values was determined by paired *t*-tests. Error bars indicate mean ± s.d.
(H) Images of ears from the WC009 and WC009^{NIL}. Scale bars: 1 cm.
(I) *ZmDeSI2* expression levels in the kernels of WC009 and C009^{NILs}.
(J) The Met content between WC009 and WC009^{NIL}. Statistical significance indicated by *P*-values was determined by paired *t*-tests. Error bars indicate mean ± s.d.
(K-P) Statistics for yield-related traits in WC009 and WC009^{NIL}. RN **(K)**, KNPR **(L)**, HKW **(M)**, KL **(N)**, KW **(O)**, and KT **(P)** respectively denote the number of rows per ear, number of kernels per row, weight of 100 kernels, kernel length, kernel width, and kernel thickness. Individual plants are represented by single dots (nWT = 15, n WC009^{NIL} = 15). Statistical significance indicated by *P*-values was determined by paired *t*-tests. Error bars indicate mean ± s.d.

1292
1293 **Figure 7. A proposed model of the molecular basis for the relationship between**
1294 ***ZmDeSI2* haplotypes and kernel Met content.** ZmDeSI2^{Hap1} exhibits a high degree
1295 of promoter activity and its transcription is positively regulated by ZmWRKY105,
1296 leading to high levels of gene expression. ZmDeSI^{Hap1} reduces the SUMOylation of
1297 ZmSIR, destabilizing this protein and limiting its accumulation, which coincides with
1298 a reduction in kernel Met content. Owing to the loss of a segment of the promoter region,
1299 ZmDeSI2^{Hap2} exhibits decreased overall promoter activity and cannot be positively
1300 regulated by ZmWRKY105 such that it is expressed at lower levels. This, in turn,
1301 weakens the deSUMOylation of ZmSIR. The enhanced SUMOylation of ZmSIR
1302 stabilizes this protein such that it accumulates, coinciding with an increase in maize
1303 kernel Met content.
1304

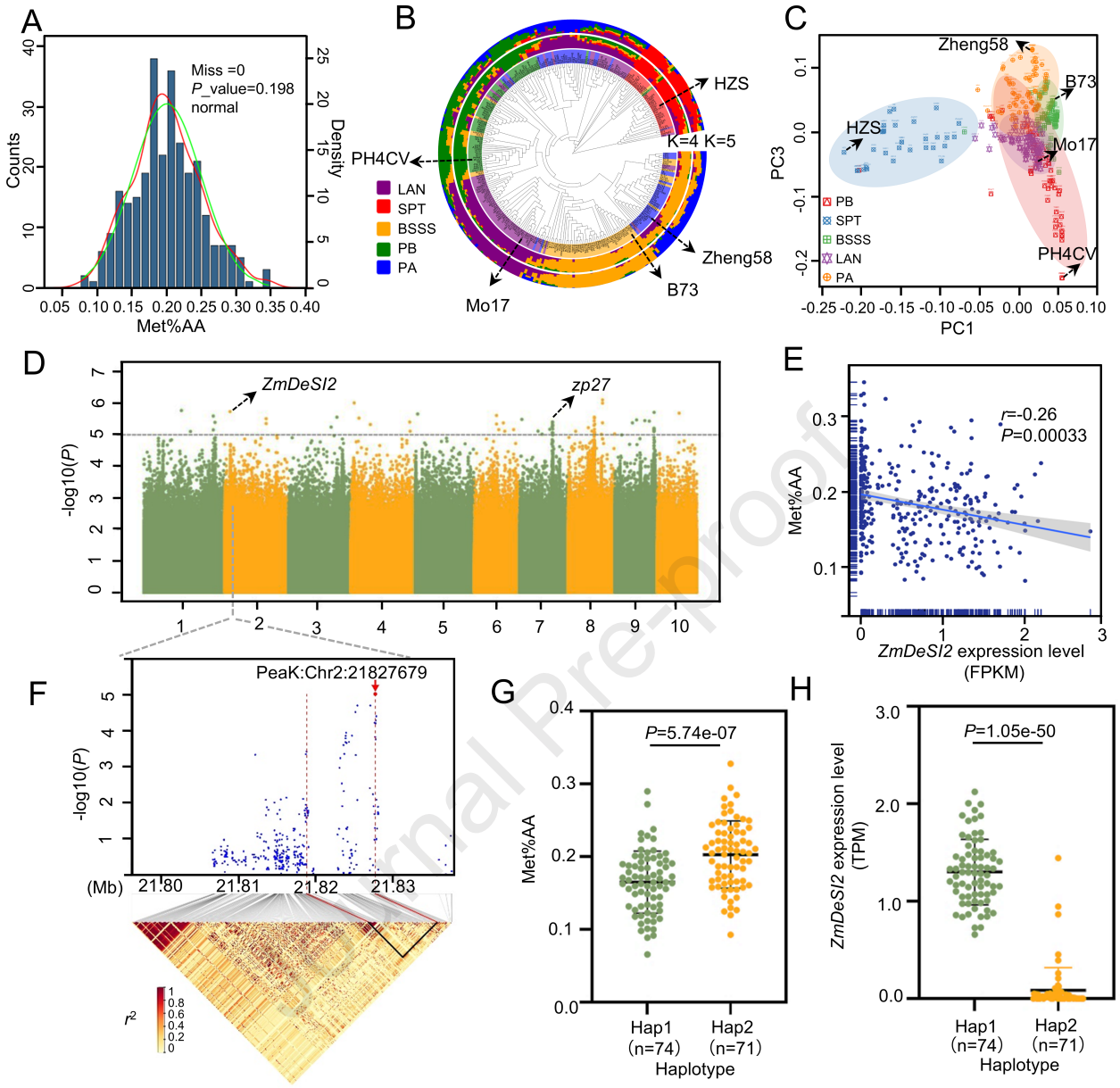
A
Miss =0
P_value=0.198
normal
Counts
Density
Met%AA
B
HZS
K=4 K=5
PH4CV
LAN
SPT
BSSS
PB
PA
Zheng58
B73
Mo17
C
Zheng58
B73
HZS
Mo17
PH4CV
PB
SPT
BSSS
LAN
PA
PC3
PC1
D
ZmDeSI2
zp27
-log10(P)
E
r=-0.26
P=0.00033
Met%AA
ZmDeSI2 expression level
(FPKM)
F
PeaK:Chr2:21827679
-log10(P)
(Mb)
r2
G
P=5.74e-07
Met%AA
Hap1
(n=74)
Hap2
(n=71)
Haplotype
H
P=1.05e-50
ZmDeSI2 expression level
(TPM)
Hap1
(n=74)
Hap2
(n=71)
Haplotype

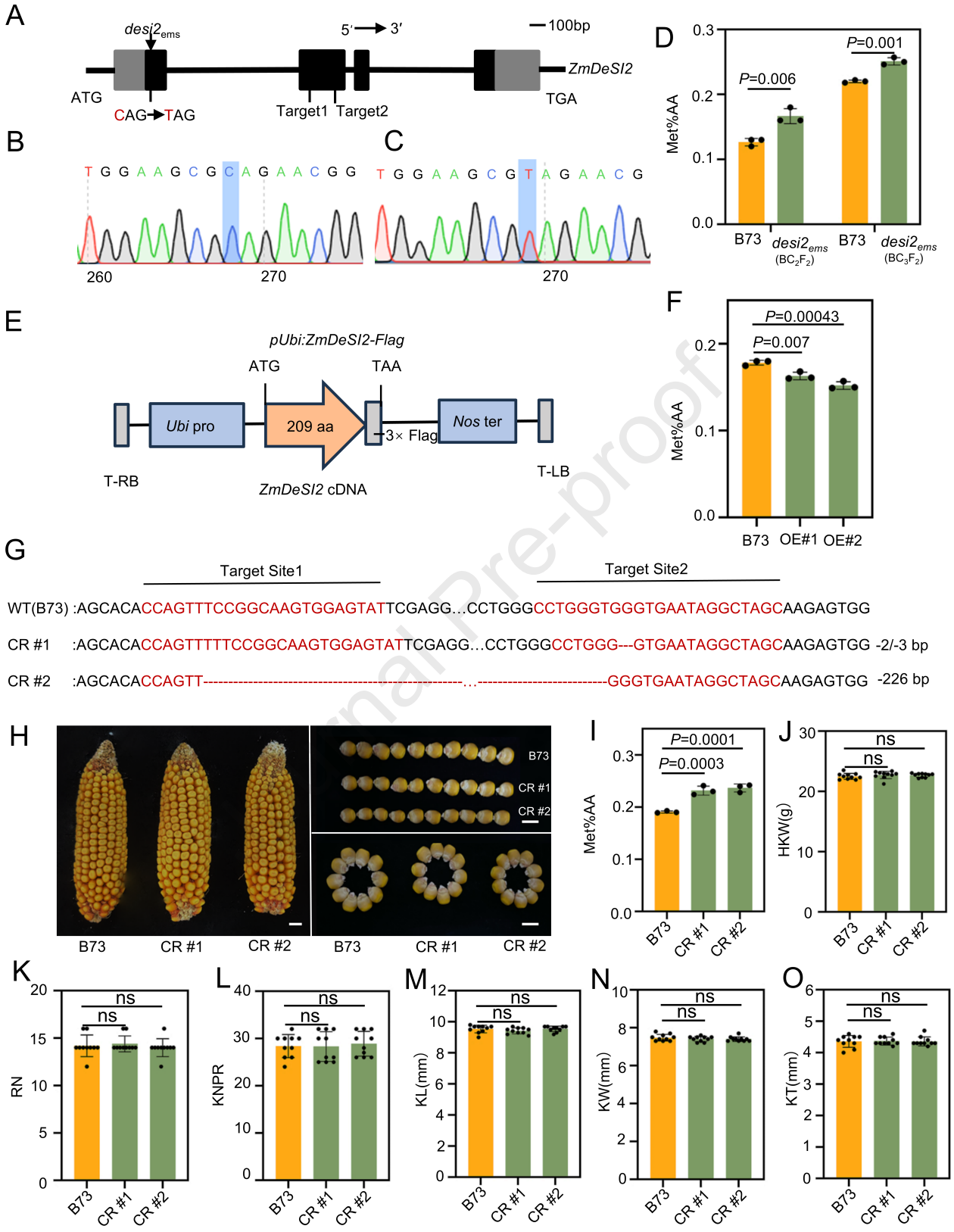
A
desi2ems
5′ → 3′
100bp
ZmDeSI2
ATG
CAG→TAG
Target1 Target2
TGA
B
C
260
270
270
D
P=0.006
P=0.001
Met%AA
B73
desi2ems (BC2F2)
B73
desi2ems (BC3F2)
E
pUbi:ZmDeSI2-Flag
ATG
TAA
Ubi pro
209 aa
3× Flag
Nos ter
T-RB
ZmDeSI2 cDNA
T-LB
F
P=0.00043
P=0.007
Met%AA
B73 OE#1 OE#2
G
Target Site1
Target Site2
WT(B73) :AGCACACCAGTTTCCGGCAAGTGGAGTATTCGAGG…CCTGGGCCTGGGTGGGTGAATAGGCTAGCAAGAGTGG
CR #1 :AGCACACCAGTTTTTCCGGCAAGTGGAGTATTCGAGG…CCTGGGCCTGGG---GTGAATAGGCTAGCAAGAGTGG -2/-3 bp
CR #2 :AGCACACCAGTT----------…----------GGGTGAATAGGCTAGCAAGAGTGG -226 bp
H
B73
CR #1
CR #2
I
P=0.0001
P=0.0003
Met%AA
J
ns
ns
HKW(g)
K
ns
ns
RN
L
ns
ns
KNPR
M
ns
ns
KL(mm)
N
ns
ns
KW(mm)
O
ns
ns
KT(mm)

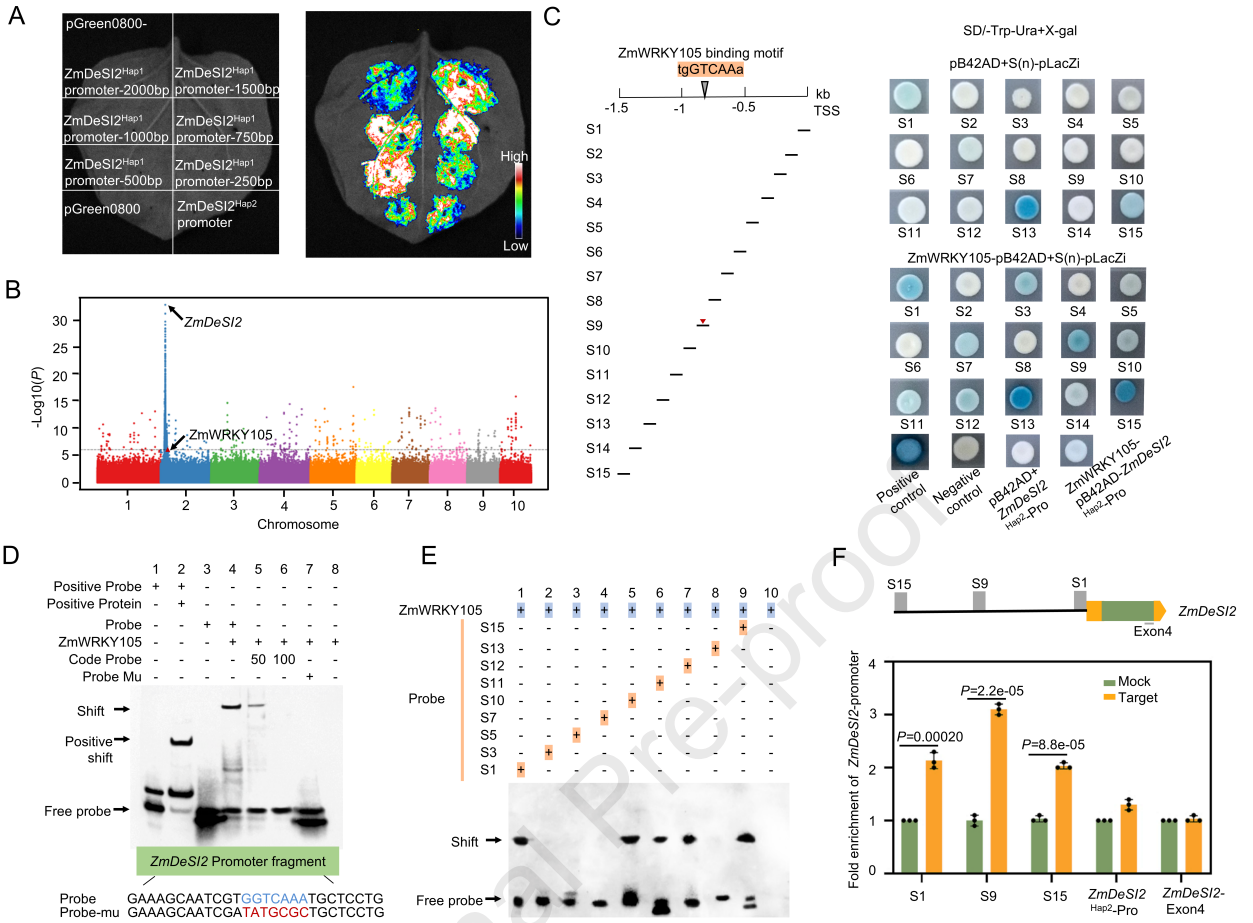
A
pGreen0800-
ZmDeSI2Hap1 promoter-2000bp
ZmDeSI2Hap1 promoter-1500bp
ZmDeSI2Hap1 promoter-1000bp
ZmDeSI2Hap1 promoter-750bp
ZmDeSI2Hap1 promoter-500bp
ZmDeSI2Hap1 promoter-250bp
pGreen0800
ZmDeSI2Hap2 promoter
High
Low
B
ZmDeSI2
ZmWRKY105
-Log10(P)
Chromosome
C
ZmWRKY105 binding motif
tgGTCAAa
kb
TSS
SD/-Trp-Ura+X-gal
pB42AD+S(n)-pLacZi
ZmWRKY105-pB42AD+S(n)-pLacZi
Positive control
Negative control
pB42AD+ ZmDeSI2 Hap2-Pro
ZmWRKY105-pB42AD-ZmDeSI2 Hap2-Pro
D
Positive Probe
Positive Protein
Probe
ZmWRKY105
Code Probe
Probe Mu
Shift
Positive shift
Free probe
ZmDeSI2 Promoter fragment
Probe GAAAGCAATCGTGGTCAAATGCTCCTG
Probe-mu GAAAGCAATCGATATGCGCTGCTCCTG
E
ZmWRKY105
Probe
Shift
Free probe
F
ZmDeSI2
Exon4
Mock
Target
P=0.00020
P=2.2e-05
P=8.8e-05
Fold enrichment of ZmDeSI2-promoter
S1
S9
S15
ZmDeSI2 Hap2-Pro
ZmDeSI2-Exon4
G
CPB+pGreen0800-ZmDeSI2Hap1promoter
CPB-ZmWRKY105+pGreen0800-ZmDeSI2Hap1promoter
CPB+pGreen0800-ZmDeSI2Hap2promoter
CPB-ZmWRKY105+pGreen0800-ZmDeSI2Hap2promoter
High
Low
H
Effecter
35S promoter
GFP
NOS
ZmWRKY105
Reporter
REN
ZmDeSI2Hap1-promoter
ZmDeSI2Hap2-promoter
LUC
I
P=1.0e-05
P = 0.423
LUC/REN
J
P=0.000433
Relative expression of ZmDeSI2
B73
wrky105
K
P=3.3e-07
Met%AA
B73
wrky105

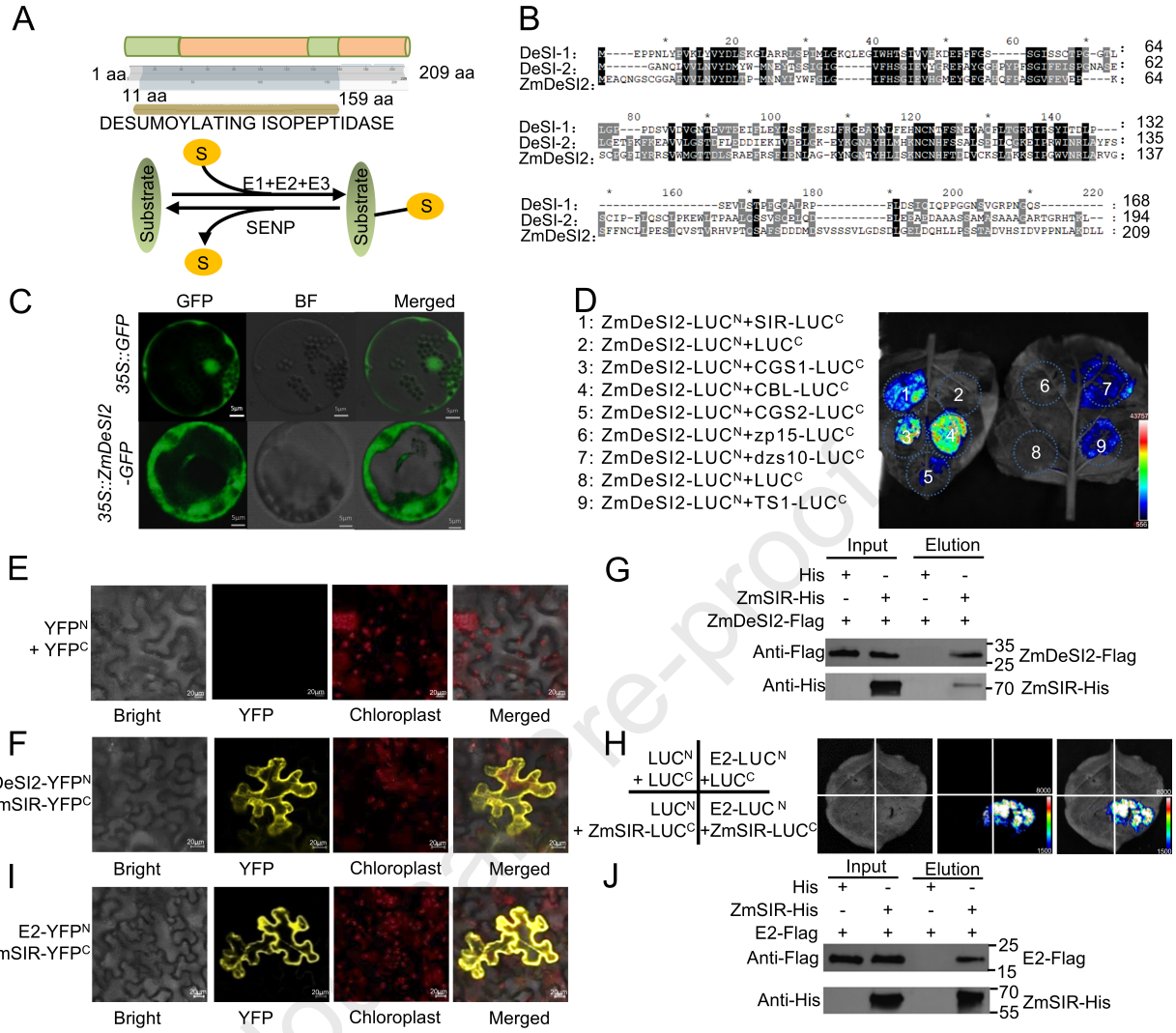
A
1 aa
209 aa
11 aa
159 aa
DESUMOYLATING ISOPEPTIDASE
S
E1+E2+E3
Substrate
SENP
B
DeSI-1:
DeSI-2:
ZmDeSI2:
C
GFP
BF
Merged
35S::GFP
35S::ZmDeSI2 -GFP
D
1: ZmDeSI2-LUCN+SIR-LUCC
2: ZmDeSI2-LUCN+LUCC
3: ZmDeSI2-LUCN+CGS1-LUCC
4: ZmDeSI2-LUCN+CBL-LUCC
5: ZmDeSI2-LUCN+CGS2-LUCC
6: ZmDeSI2-LUCN+zp15-LUCC
7: ZmDeSI2-LUCN+dzs10-LUCC
8: ZmDeSI2-LUCN+LUCC
9: ZmDeSI2-LUCN+TS1-LUCC
E
YFPN + YFPC
Bright
YFP
Chloroplast
Merged
F
ZmDeSI2-YFPN + ZmSIR-YFPC
I
E2-YFPN + ZmSIR-YFPC
G
Input
Elution
His
ZmSIR-His
ZmDeSI2-Flag
Anti-Flag
Anti-His
ZmDeSI2-Flag
ZmSIR-His
H
LUCN + LUCC
E2-LUCN +LUCC
LUCN + ZmSIR-LUCC
E2-LUCN +ZmSIR-LUCC
J
E2-Flag
Anti-Flag
Anti-His
E2-Flag
ZmSIR-His

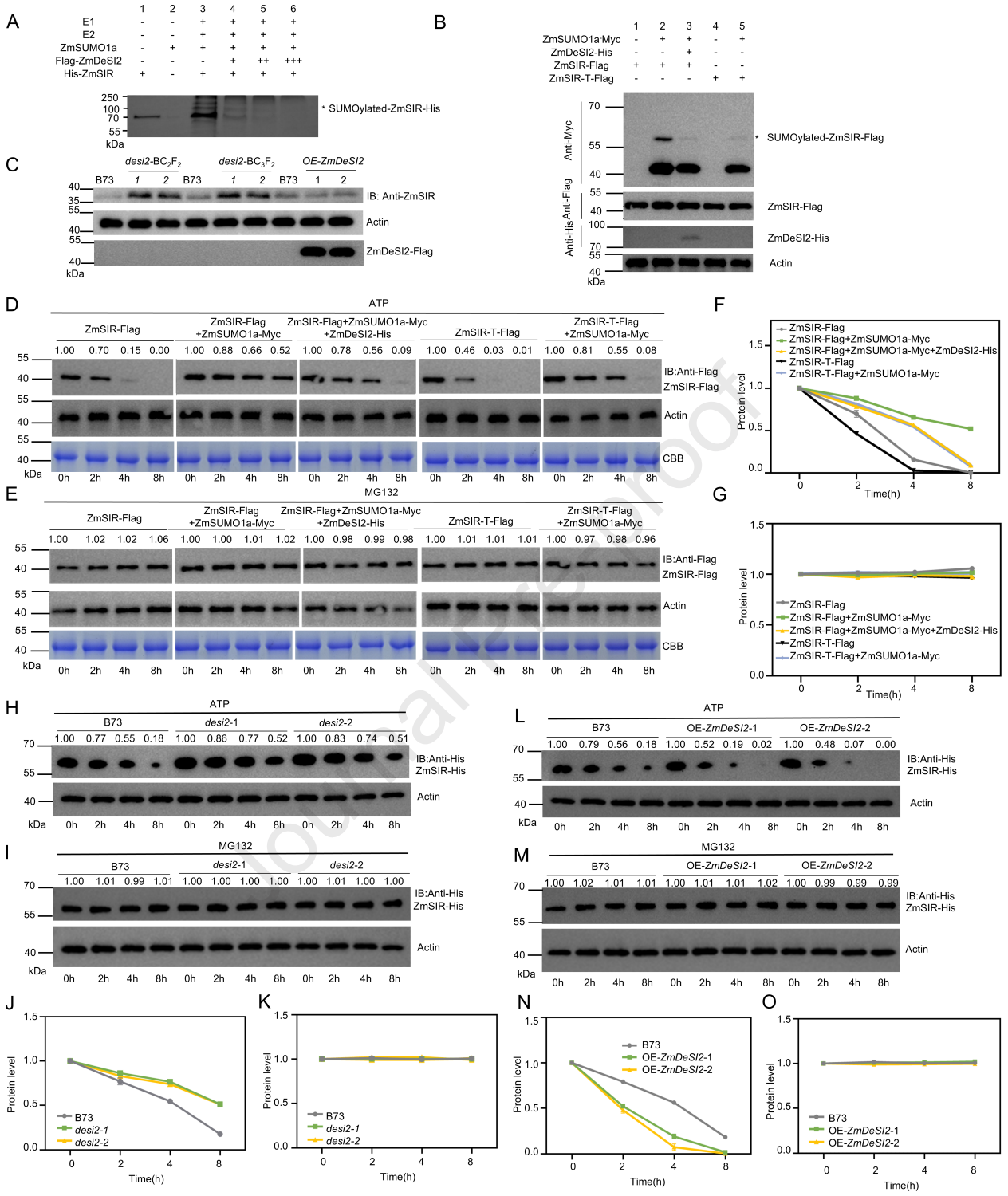
A
1 2 3 4 5 6
E1 - - + + + +
E2 - - + + + +
ZmSUMO1a - + + + + +
Flag-ZmDeSI2 - - - + ++ +++
His-ZmSIR + - + + + +
250
100
70
55
kDa
* SUMOylated-ZmSIR-His
B
1 2 3 4 5
ZmSUMO1a-Myc - + + - +
ZmDeSI2-His - - + - -
ZmSIR-Flag + + + - -
ZmSIR-T-Flag - - - + +
Anti-Myc
Anti-Flag
Anti-His
* SUMOylated-ZmSIR-Flag
ZmSIR-Flag
ZmDeSI2-His
Actin
C
desi2-BC2F2
desi2-BC3F2
OE-ZmDeSI2
B73 1 2 B73 1 2 B73 1 2
IB: Anti-ZmSIR
Actin
ZmDeSI2-Flag
D
ATP
ZmSIR-Flag
ZmSIR-Flag +ZmSUMO1a-Myc
ZmSIR-Flag+ZmSUMO1a-Myc +ZmDeSI2-His
ZmSIR-T-Flag
ZmSIR-T-Flag +ZmSUMO1a-Myc
1.00 0.70 0.15 0.00
1.00 0.88 0.66 0.52
1.00 0.78 0.56 0.09
1.00 0.46 0.03 0.01
1.00 0.81 0.55 0.08
IB:Anti-Flag ZmSIR-Flag
Actin
CBB
0h 2h 4h 8h
E
MG132
1.00 1.02 1.02 1.06
1.00 1.00 1.01 1.02
1.00 0.98 0.99 0.98
1.00 1.01 1.01 1.01
1.00 0.97 0.98 0.96
F
ZmSIR-Flag
ZmSIR-Flag+ZmSUMO1a-Myc
ZmSIR-Flag+ZmSUMO1a-Myc+ZmDeSI2-His
ZmSIR-T-Flag
ZmSIR-T-Flag+ZmSUMO1a-Myc
Protein level
Time(h)
G
H
ATP
B73
desi2-1
desi2-2
1.00 0.77 0.55 0.18
1.00 0.86 0.77 0.52
1.00 0.83 0.74 0.51
IB:Anti-His ZmSIR-His
Actin
I
MG132
1.00 1.01 0.99 1.01
1.00 1.00 1.00 1.00
1.00 1.01 1.00 1.00
L
OE-ZmDeSI2-1
OE-ZmDeSI2-2
1.00 0.79 0.56 0.18
1.00 0.52 0.19 0.02
1.00 0.48 0.07 0.00
M
1.00 1.02 1.01 1.01
1.00 1.01 1.01 1.02
1.00 0.99 0.99 0.99
J
K
N
O
B73
desi2-1
desi2-2
OE-ZmDeSI2-1
OE-ZmDeSI2-2

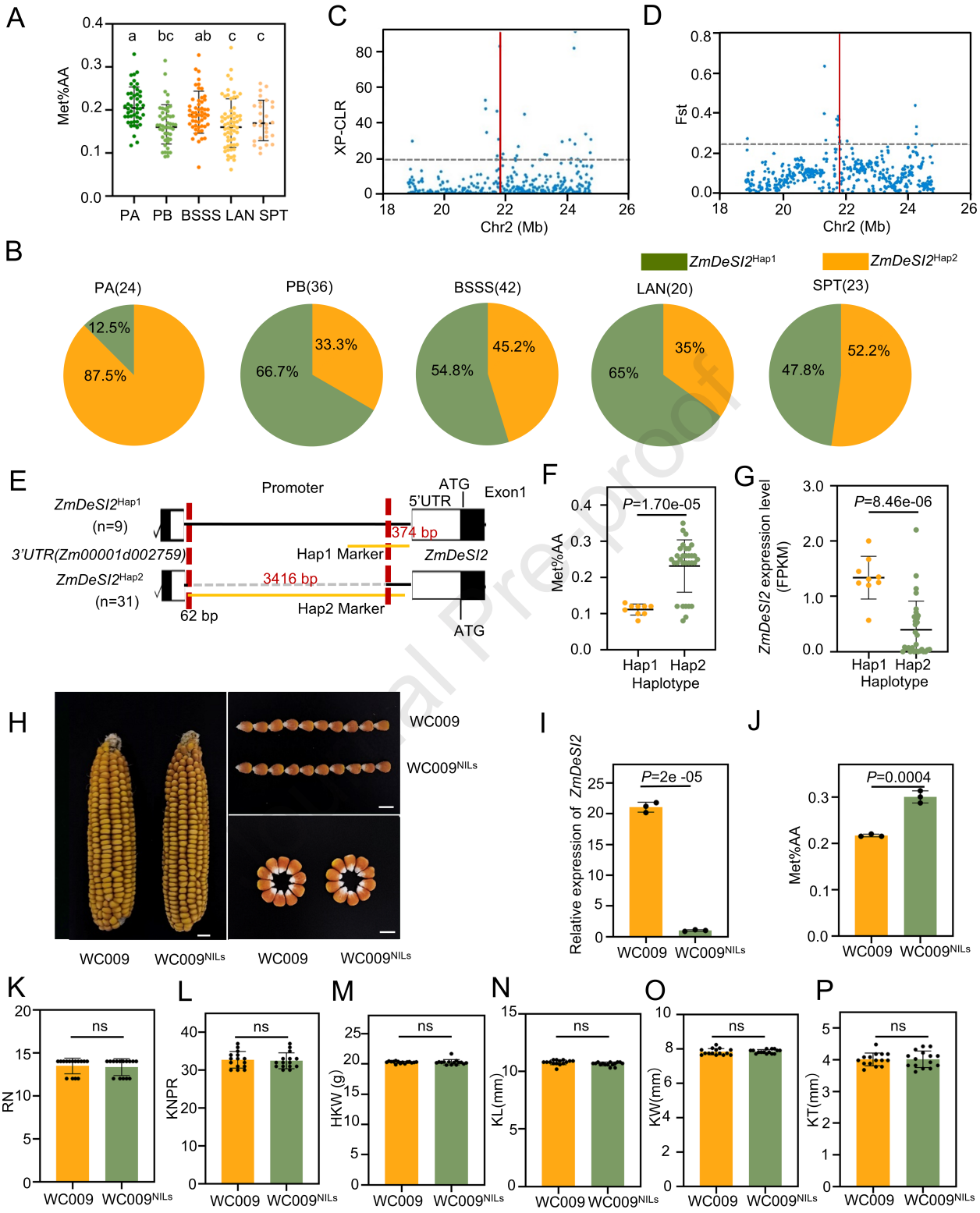
A
Met%AA
a bc ab c c
PA PB BSSS LAN SPT
C
XP-CLR
Chr2 (Mb)
D
Fst
Chr2 (Mb)
B
ZmDeSI2Hap1
ZmDeSI2Hap2
PA(24)
12.5%
87.5%
PB(36)
33.3%
66.7%
BSSS(42)
45.2%
54.8%
LAN(20)
35%
65%
SPT(23)
52.2%
47.8%
E
Promoter
ATG
5'UTR
Exon1
ZmDeSI2Hap1
(n=9)
374 bp
3'UTR(Zm00001d002759)
Hap1 Marker
ZmDeSI2
ZmDeSI2Hap2
(n=31)
3416 bp
62 bp
Hap2 Marker
ATG
F
P=1.70e-05
Met%AA
Hap1 Hap2
Haplotype
G
P=8.46e-06
ZmDeSI2 expression level (FPKM)
Hap1 Hap2
Haplotype
H
WC009
WC009NILs
WC009 WC009NILs WC009 WC009NILs
I
P=2e -05
Relative expression of ZmDeSI2
WC009 WC009NILs
J
P=0.0004
Met%AA
WC009 WC009NILs
K
ns
RN
WC009 WC009NILs
L
ns
KNPR
WC009 WC009NILs
M
ns
HKW (g)
WC009 WC009NILs
N
ns
KL(mm)
WC009 WC009NILs
O
ns
KW(mm)
WC009 WC009NILs
P
ns
KT(mm)
WC009 WC009NILs